[Frontiers in Bioscience 17, 1551-1581, January 1, 2012]

The osteon: the micromechanical unit of compact bone

Maria-Grazia Ascenzi[1], Allison K. Roe[1]

[1]*UCLA,Orthopaedic Hospital Department of Orthopaedic Surgery, University of California at Los Angeles*

TABLE OF CONTENTS

1. ABSTRACT

The research techniques available for investigation of secondary osteons in human bone enable establishment of their biological composition and quantification of their mechanical properties. Further, the data generated through current research techniques facilitate studies on the significance of osteons in normal and pathological conditions, including via multi-scale modeling conducted with a view of building realistic models of virtual bone, suitable for applications from orthopaedic challenges to endocrine disorders. The understanding of the biomechanical function of the osteon requires clarification of the molecular-cellular processes that form, maintain and remodel the osteon and affect the mechanical function. In turn, the mechanical function affects the biology of the osteon. In retrospective, the investigation of osteons has focused on the unraveling of the complex combination of elementary components to discern the major factors that define the mechanical behavior. The micro-structural environment that leads to macroscopic fracture remains unclear. Arrangement, distribution and quality of the elementary components may participate in fracture risk. The latest results underline the fundamental role of the orientation of collagen type I and of carbonated hydroxyapatite crystallites.

2. INTRODUCTION

Bone presents a series of seemingly contradictory characteristics: rigidity, strength, toughness, flexibility and lightness. It is the concept of multi-scale structure, first introduced by Petersen (1) in the 1930's, that allows for an understanding of the coexistence of such disparate properties. Well prior to Petersen, Galileo first hypothesized in the 1600's that the macro-structure needed reinforcements along the axis of long bones of large animals to avoid that the shaft collapse under its own weight (2). Petersen's further insight as to bone's multi-scale structure synthesizes observations that bone shows structural arrangements that depend on the magnification at which they are observed or measured, a characteristic that became apparent over several centuries of improvement in microscopy resolution. The modern study of bone microstructure began in the 1940's with the studies pursued by the School of Anatomy in Bologna (3).

This chapter discusses the micro-structure of compact adult human bone that forms the Haversian system, and whose basic unit is the secondary osteon

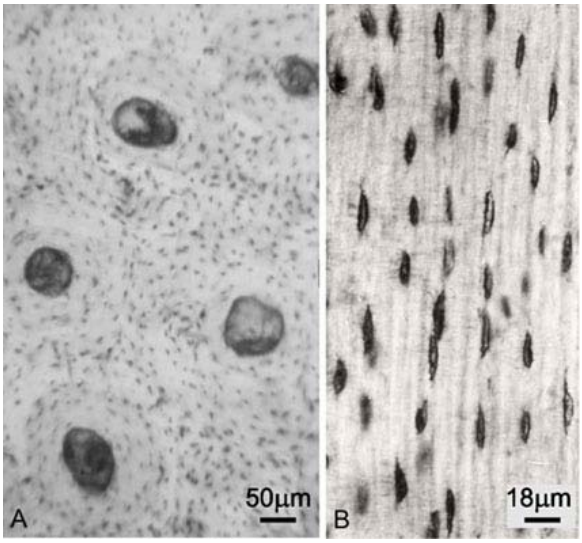

Figure 1. Haversian system. Secondary osteons are viewed on (a) transverse section by transmitted light; and on (b) longitudinal section by reflected light. Osteocyte lacunae (appearing black) form circular patterns on transverse section and longitudinal patterns on longitudinal sections.

(Figure 1). The focus of this chapter is the osteon's mechanical function. During the continuous process of bone remodeling, the secondary osteon forms around a vascular canal, also known as a Haversian canal. The secondary osteon is composed of layers, called lamellae, the structure of which has been an open question since van Leeuwenhoek first observed them in the late 1600's (4). There are two distinct hypotheses on the structural composition of the lamella. Both recognize that there are two types of lamellae that compose the osteons. The first hypothesis is that the two types of lamellae differ in orientation of the main elementary components of bone tissue, namely collagen fibrils and carbonated hydroxyapatite crystallites (5, 6, 7, 8, 9, 10, 11, 12, 13, 14). This hypothesis has evolved in time to become increasingly sophisticated. Gebhardt in the 1900's was the first to theorize a difference in orientation of collagen bundles with a spiral arrangement, either clockwise or counterclockwise, which may vary through an angle from 0 to 90 degrees with the osteon axis. This hypothesis has long been a model for investigating the mechanical behavior of isolated micro-structures (15, 16, 17, 18, 19, 20) and the correlations between micro- and macro-mechanics in compact bone (21). The second hypothesis is that the two lamellar types differ in the relative densities of the elementary components and in particular of collagen (22, 23, 24, 25, 26, 27, 28, 29, 30). The current chapter addresses the experimental results of the research on osteons and their lamellar components, and the related evolution, and ultimate intersection, of the micro-biomechanical hypotheses.

Section 3 summarizes the understanding of osteon composition. Section 4 describes the experimental techniques that are available to investigate the basic morphology of osteons. Section 5 describes the techniques for isolation of a single osteon and a single lamella and the methods to test their mechanical properties. Section 6 describes confocal and electron microscopy techniques and the results of their application to osteons. Section 7 explains the assessment of the mechanical properties of bone tissue within an osteon and its lamellae. Section 8 sets forth insights obtained from findings of collagen and apatite anisotropy within the osteon and throughout the macro-structure. Section 9 offers an overview of techniques from the fields of mathematics and engineering to aid the analysis of experimental results on bone micro-structures. The promise of interdisciplinary collaboration is explained to further the research on bone micro-structure within the multi-scale context. Section 10 addresses the open problems relative to bone micro-structure, the investigation of its elementary components and structures, and the application of such investigations to clinical challenges.

3. OSTEON COMPOSITION

This section describes the biological composition of secondary osteons. Secondary osteons were first observed under regular light microscopy to consist of cylindrical units comprising several layers called lamellae, that are generally coaxial with the axis of the Haversian (or vascular) canal around which they form (Figure 1). So-called interstitial bone fills in the space among the osteons and consists of remnants of osteons left over by the remodeling process. In male young adults free of metabolic bone disease, the osteon diameter ranges between 84 and 300 micron, with a Haversian canal diameter between 11 to 68 micron and a lamellar thickness between 2 and 16 micron (3, 31, 32, 33). These morphological dimensions depend on the skeletal site of the osteon. Because the Haversian system shows morphological heterogeneity that depends on the age of the individual, skeletal site and presence or absence of systemic factors that can alter the bone tissue, well-founded studies of bone composition focus on a specific skeletal site while addressing patients or donors with similar characteristics, separating for instance adolescents, young adults, and the elderly of either sex from each other, as well as distinguishing between pre-menopausal and post-menopausal females, and specific stages of any given pathology.

The calcified tissue of bone consists of three elements: cells, organic matrix and inorganic substance. These components are dependent upon each other, as the cells are known to assemble the organic matrix and generate the organic molecules that participate in the process of calcification. About 90% of the organic matrix of bone consists of collagen. The remaining 10% consists of proteoglycans, Gla-proteins (protein attached to gamma-carboxyglutamic acid), glycoproteins and phospholipids.

Collagens are fibrous proteins with structural properties that control arrangement, assembly, integrity and mechanical properties in many living organisms. Among the large number of collagen types (fibrillar, reticular, fibril surface-associated, periodic beaded filamentous and trans-membrane; 34, 35, 36), type I collagen belongs to the fibrillar type and comprises most of the bone matrix. Three

polypeptide chains coiled in a left-handed helix form a collagen molecule, 280-300nm long (37). The collagen molecules align themselves according to a quarter-staggered arrangement with gaps between the front and back of the collagen molecules in sequence (38, 39). The fibrils show diameters of approximately 78nm. Adjacent molecules are connected to each other by intra- and intermolecular cross-links (40, 41, 42). These cross-links stabilize the structure of the collagen bundle, cause low solubility of bone collagen (43), and possibly play a part in the calcification of the collagen fibers. Because collagen is inter-dispersed through the bone matrix and therefore difficult to study independently from other components and without alteration of its structure for extraction, most of the knowledge about the structural characteristics of collagen type I arises from studies based on collagen found in undecalcified tendons and in other soft tissues, for instance skin tissues.

The bundles of type I collagen are mineralized into crystal-like configurations within a three-dimensional (3D) network (34). After the collagen is laid down by the osteoblasts, the process of calcification starts and leads to the formation of a solid, stable, crystalline inorganic phase within the organic phase. Carbonated hydroxyapatite crystals generally parallel collagen bundles (44). The bone turnover rate determines bone age and age-dependent properties of bone (45). The density and composition of the collagen fibrils in the bone matrix vary according to site and types of bone. Collagen fibrils are most dense in the compact bone of the diaphyses because fibrils are condensed together and assembled in an ordered layout called parallel-fibered or lamellar bone. In contrast, fibrils are aligned randomly in woven bone. They intertwine in a sporadic design and give rise to a large interfibrillary space (46), as opposed to the small interfibrillary space in lamellar bone. Therefore, woven bone has a larger portion of non-collagenous material than lamellar bone (47, 48). The orientation of collagen fibrils is important because differences in the amount of space between fibers allows varied amounts of non-collagenous material and because the orientation has implications for bone's mechanical properties (21, 49).

Non-collagenous components of the bone matrix are important because they affect bone formation rate and collagen bundle spacing, even though they make up a smaller fraction of compact bone (50, 51, 52, 53, 54, 55, 56, 57, 58, 59, 60, 61). Different types of bone show varying amounts of these components, which are more abundant in bone tissues with loose collagen fibrils (62, 63). Proteoglycans are the most abundant non-collagenous components of bone and generally entrapped in the calcified matrix. Decorin is a specific type of proteoglycan which regulates collagen fibrillogenesis (64), inhibits calcification and is associated with type I collagen (65). Biglycan, aggrecan, versican, perlecan and fibromodulin are additional types of proteoglycan less abundant in the bone matrix than decorin.

Osteoblasts, osteocytes and osteoclasts are the cells present in the bone tissue. Osteoblasts synthesize collagen and are therefore considered bone forming cells. Osteocytes make up over 90% of all bone cells and are osteoblasts that become entrapped in the matrix that they produce (66). They are hypothesized to have a sensory role (67, 68, 69) for mechanical loading. Osteoclasts are primarily responsible for bone resorption. The functional interplay of this type of cells is complex, with the three-cell types affecting each other's function (70, 71). Osteocalcin (OC) and matrix Gla-protein (MGP) are two important types of Gla-proteins. OC is restricted to the bone matrix and is assembled by osteoblast cells (72, 73, 74). It requires vitamin K for synthesis, and shows calcium-binding characteristics that help its interaction with hydroxyapatite (75). OC's close interaction with hydroxyapatite is hypothesized to inhibit growth of crystalline hydroxyapatite and to guide its shape and size (76). OC is present at higher levels in cortical than trabecular bone (77, 78) and has been regarded as a local calcification regulator. OC is synthesized at the earliest stage of calcification and is the only non-collagenous protein confined to bone cells and calcified matrix (79). Its function is difficult to determine and has never been clearly defined. Circulating OC is nevertheless involved in bone turnover (54, 80). However, it has also been shown that OC does not interact with lipid-induced hydroxyapatite formation and has no impact on lipid-induced calcification (81). MGP is similar to OC in that it depends on vitamin K for synthesis and it contains Gla (82). Further, MGP negatively regulates calcification (83, 84, 85, 86). Evolutionarily, it is possible that MGP and OC arose due to gene duplication and then divergent evolution due to the similarity in protein sequences (87).

Bone matrix also contains glycoproteins. Glycoproteins that are highly phosphorylated are called phosphoproteins. Different types of bone phosphoproteins are osteonectin, osteopontin, bone sialoprotein, dentin matrix protein 1, matrix extracellular phosphoglycoprotein and acidic glycoprotein-75. Glycoproteins containing glutamic, aspartic and sialic acids are called acidic glycoproteins (88). In order for glycoproteins to become soluble, the bone tissue needs to be decalcified (52, 53, 89, 90). In fact, glycoproteins are buried in the inorganic elements of the bone matrix, which founds the belief that they affect bone calcification (55, 56, 89, 91, 92).

While bone tissue of human and other animals shares many characteristics, research shows that differences exist between human bone and the bone of other mammals, such as monkeys, horses, calves, sheep dogs, rabbits, dogs generically, and ferrets, all of which show osteon remodeling (93, 94, 95, 96, 97). Osteonal remodeling is absent in rat and mouse bone (98).

4. TECHNIQUES TO ASSESS BASIC MORPHOLOGY

A principal focus of research in the late 1940's and 1950's was the identification of the parameters that can explain the heterogeneity of the Haversian system. Polarized light microscopy was chosen because it provides information on organization of components of a translucent material. Further, because bone remodeling targets the

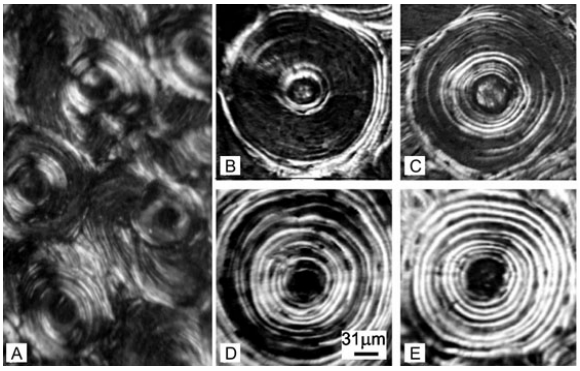

Figure 2. Extinct and bright birefringence of CPL. (a) 70 micron-thin transverse section at femoral mid-shaft at Figure 1a is viewed under CPL. (b-e) Percent area and distribution of extinct and bright birefringence vary in single osteon: example of single osteons with (b) 3%, (c) 20%, (d) 60% and (e) 90% bright percent area. Reproduced with permission from ref #116.

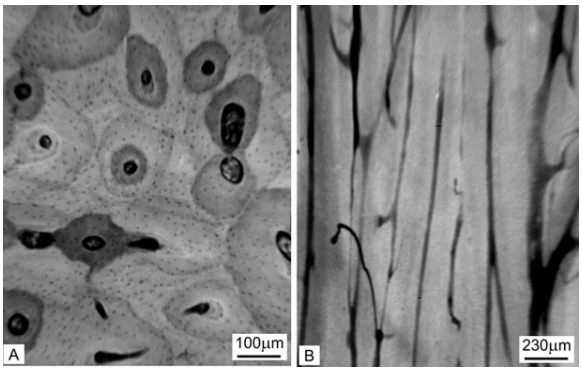

Figure 3. High-resolution micro-X-ray. (a) Transverse and (b) longitudinal section of femoral mid-shaft show a distribution of grey shades (c) where light grey corresponds to final stages of calcification and darker grey correspond to initial stages of calcification. Reproduced with permission from ref #116.

osteon unit, the need became apparent to develop radiological instrumentation that would afford a resolution high enough to allow detection of the degree of calcification within the single osteon. The morphological investigations that were carried out then and subsequently have been implemented with increasing refinement on bone sections and on isolated specimens of either osteons or lamellae. In combination, the techniques of polarized light microscopy and high resolution micro-X-ray have allowed assessment of two fundamental micro-structural variables: (i) collagen and apatite anisotropy and (ii) degree of osteon calcification.

4.1.Polarized light

Polarization of light has been used in conjunction with transmitted light microscopy to detect anisotropy of bone since the 1950's (99). Circularly polarized light (CPL) is obtained by means of two crossed Nicol's prisms and two quarter lambda retardation plates. Of the Nicol's prisms, the polarizer is situated between the light source and the bone specimen, and the analyzer is situated above the specimen. The first quarter lambda plate oriented at 45 to 225 degrees is situated between the polarizer and the specimen. The second quarter lambda plate, oriented at 135 to 315 degrees, is situated between the specimen and the analyzer (100, 101).

The crossed Nicol's prisms induce propagation of light on perpendicular planes whose common axis is the direction of propagation. The presence/absence of the first quarter lambda plate differentiates between CPL and linear polarized light. The bright signal of CPL corresponds to the bright signal for all rotations of the specimen on the microscope stage under linear polarization and similarly so for the extinct signal. The second quarter lambda plate removes the extinct Maltese cross effect due to the extinct appearance of structural elements aligned parallel to the transmission axis of the Nicol's prisms.

Extinct and bright signals of CPL are due to birefringence of collagen and in a minor way to hydroxyapatite. This can be checked by comparing the distribution of extinct and bright signals before and after calcification of a bone specimen. Extinction of light is indicative of collagen bundles preferentially parallel to the direction of the propagation of light, while brightness is indicative of collagen generally forming large angles, including transverse collagen, with the direction of propagation. Therefore the CPL signal depends on the orientation of the section: regions that appear extinct on sections transverse to the Haversian system general direction appear bright on longitudinal section. Conversely, regions that appear bright on section transverse to the Haversian system general direction appear extinct on longitudinal section.

Osteons can be classified in terms of appearance under CPL. Throughout this chapter we refer to extinct and bright birefringence of osteons in transverse section (Figure 2). A completely extinct osteon has never been observed. The so-called extinct osteon shows 96 to 97% extinction corresponding to 3 to 4% percent brightness). The so-called bright osteon is 100% bright. The so-called alternate osteon shows alternation of bright and extinct lamellae.

4.2. High-resolution micro-X-ray

The degree of calcification is assessed with a micro-focus microradiograph MCR 3000 (Ital-Structures, Riva del Garda-Trento, Italy) and high-resolution film such as Kodak 649 film (now discontinued), or 1A plates from Microchrome Technology, Inc or VRP-N plates from Slavich with 2000 to 3000 lines/mm (26, 102, 103).

To calibrate and allow quantification of calcium, the bone specimen is micro-X-rayed together with an aluminum scale consisting of four segments of increasing thickness, because aluminum, calcium and phosphorous absorb x-rays with a comparable coefficient within the energy range used by the microradiograph (104). The darker grey shades on the micro-X-ray correspond to initial stages of calcification and the lighter grey shades to final stages of calcification (Figure 3). Haversian canals and resorption lacunae appear black on

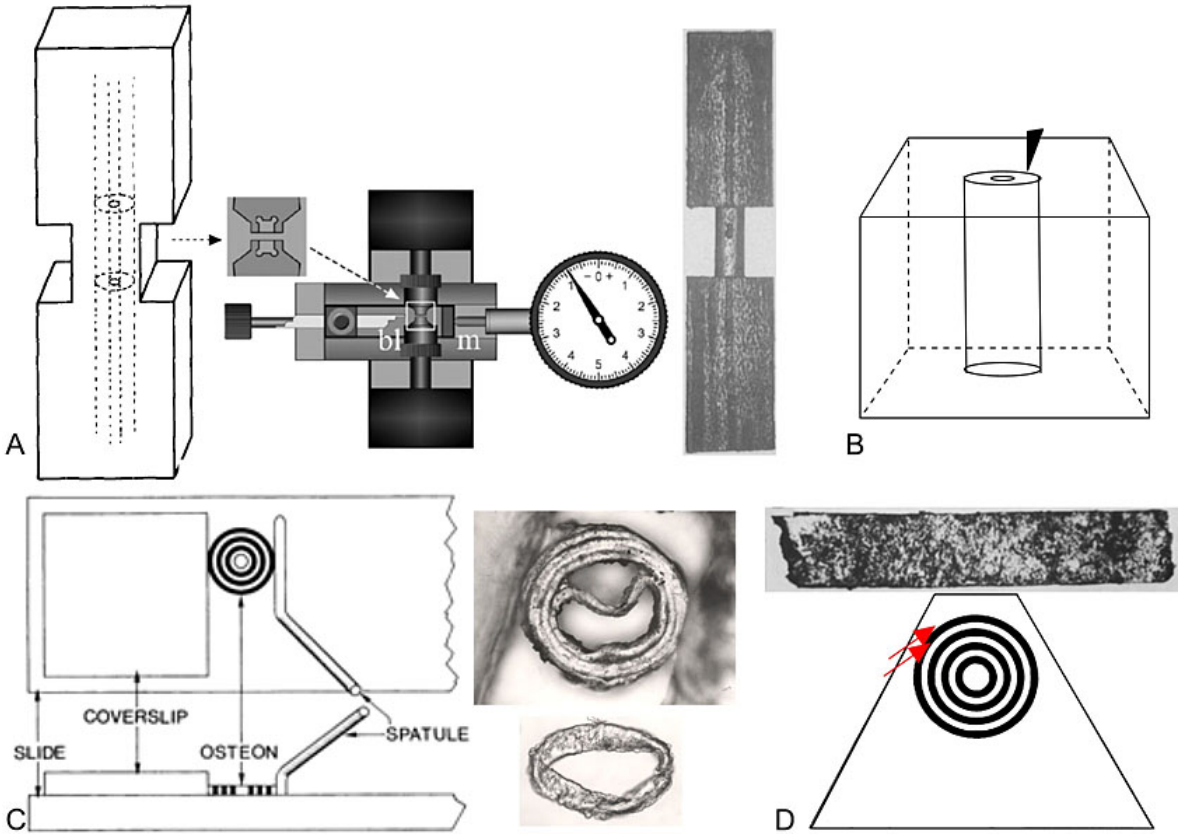

Figure 4. Preparation of specimens. (a) A specimen of single osteon is isolated as a cylinder with lugs. A boxed specimen is cut with a micro-lathe around a Haversian canal whose length is on the order of 500-535 micron to avoid Volkman's canals that would create large discontinuities in the specimens and affect mechanical testing. The boxed specimen is placed in the enlarged rectangular pocket of the schematic of the micro-lathe. The advancing blade (bl), controlled by a micrometer (m), serves to establish the diameter of the cylindrical portion of the specimen. (b) This is a diagram of a cylindrical specimen that can be isolated on a section transverse to the Haversian canal with a micro-mill (in black). In both (a) and (b) the specimen is cut around the Haversian canal whose axial is aligned with the axis of the cylinder. (c) Isolation of extinct single lamella in carried out by diametric compression of alternate osteon and shown with a diagram of two views of the device. (d) Extinct or bright lamella can be isolated by excision on a trapezoid cut around an osteon from a transverse section shown in a diagram. The bottom part of the trapezoid is glued to a glass slide for holding while the excision is carried out with a micro-blade along the outer-most lamella (red arrows) under CPL. Because of the holding requirement, up to two-thirds of the circumferential length of the lamella can be isolated. Reproduced with permission from refs #19, 44, 109, 118.

the micro-X-ray. Interstitial bone appears, in general, whiter than osteons, indicating higher calcification, explained by the older tissue age. Because of the 1 micron resolution, the cement lines, whose thickness ranges between 1 and 2 micron, are visible at the interface between osteons and interstitial bone. Their dark appearance suggests low calcification. The degree of calcification in cement lines is nevertheless a matter of divergent views (105, 106, 107).

5. MECHANICAL TESTING OF SINGLE OSTEON AND OF SINGLE LAMELLA

Because the mechanical behavior of a specimen depends on its composition, specimens are chosen of specific types under CPL (section 4.1) and at specific degree of calcification as established by the micro-X-ray method described (section 4.2). Because the mechanical behavior of a specimen depends also on its dimensions and shape, the issue of isolating osteons of same dimension and shape presents itself. The quasi-static mechanical testing described below requires isolation of single osteons, for which preparation techniques were developed in the 1960's and 1970's. Single osteon specimens have been prepared with a cylindrical shape for compression, pin-test, bending, shear (Figure 4a), and with a cylindrical shape connected to two lugs, one per end, for tension, torsion, cyclic tension-compression, cyclic torsion (Figure 4b). In either case, the cylindrical shape was chosen coaxial to the vascular canal. In specific instances hemi-diametral osteon sections have also been tested. Single lamellar specimens have been prepared (Figure 4c) and tested in tension. Mechanical tests have been performed on both dry specimens and on specimens wetted with either saline solution or distilled water, which replicate physiological conditions. Only results obtained on hydrated specimens are reported here

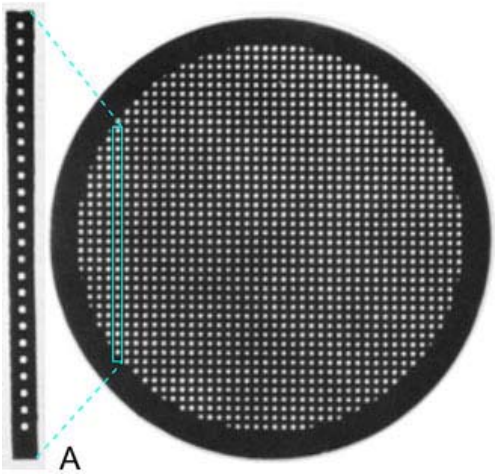

Figure 5. Monotonic tension of single lamella. (a) A copper grid for electron microscopy is cut to obtain supports to attach the specimen to the extensometer. (b-c) Lamellar specimen attached to its supports (b) before and (a) after tensional loading along the lamellar length. Reproduced with permission from ref #109.

5.1. Techniques to isolate single osteons

Protocols to prepare a single osteon specimen around the vascular canal were developed in the late 1960's. The site for specimen isolation needs to be chosen around a straight Haversian canal and away from Volkman's canals. Consequently, the longitudinal axis of the specimen needs to coincide with the axis of the Haversian canal and the Haversian canal length of the specimen cannot exceed 520-530 micron. To obtain specimens with lugs (Figure 4a), longitudinal sections were cut from the long bone shaft, with a thickness that was slightly larger than the osteon diameter. Such sections were micro-X-rayed to choose osteons with specific degree of calcification (section 4.2). The sections were then observed by CPL to select specific osteon anisotropy. Because the overlapping of lamellae beyond 100 micron thickness may affect the CPL signal, the appearance of the specimen under CPL needs to be confirmed after testing by isolating thinner transverse sections and observing them by CPL. Micro-instrumentation was developed to cut the specimens. To isolate a box shaped specimen from the longitudinal sections, a micro-mill was used where the body of a dental drill replaces the tube in the body of a microscope. The isolation of the specimen was observed with a stereo-microscope. A micro-grinding lathe was then used with the axis of the Haversian canal aligned with the rotating axis of the lathe, to obtain a cylindrical middle portion of the specimen.

To obtain cylindrical specimens (Figure 4b), sections were cut transversely to the Haversian canal's general direction. After conducting micro-x-rays to select osteons of specific degree of calcification and after observation by CPL to select specific structural anisotropy, a circular cut within the chosen osteon was made around the Haversian canal with the micro-lathe. This process produced a cylindrical specimen.

5.2. Techniques to isolate single lamellae

The lamellae that appear bright on sections transverse to the Haversian axes can be isolated by hemi-diametral compression (Figure 4c; 15); and both extinct and bright lamellae can be isolated by excision (Figure 4d; 44). Hemi-diametral light compression of a cylindrical osteon specimen causes fracture of extinct lamellae, while bright lamellae remain intact. Whole bright lamellae exit the osteon specimen in an opening telescopic fashion. The lamella is then cut along its height and carefully laid down flat under microscope observation. The second method consists in excision of lamellae. This technique is carried out on a trapezoid cut from a 70 micron thick transverse section. The bottom portion of the trapezoid is glued to a glass slide in order to hold the specimen while cutting. Approximately two-thirds of the lamellar circumferential length is isolated while the specimen is kept wet.

5.3. Monotonic tension test

Historically, hemi-diametral specimens were first tested in tension (16). Because hemi-diametral sections from alternate osteons showed abrupt changes in slope at low stresses, hemi-diametral specimens were found unsuitable to measure adequately the mechanical properties of the osteons because the specimen preparation removed the longitudinal initial stress that normally protects alternate osteons at low stresses (15). Therefore, cylindrical specimens needed to be employed.

Extinct and alternate osteons at initial and final stages of calcification were chosen to prepare cylindrical specimens endowed with lugs for this experiment. The CPL osteon type needs to be confirmed after the experiment because of the presence of the lugs. In fact, two thin sections need to be cut at each end of the cylindrical shape and viewed by CPL. The osteon specimen diameters ranged between 20 and 50 micron and the height ranged between 400 and 600 micron (33).

The transverse area of the specimen's cylindrical part was used to determine the ultimate tensile stress. A loading apparatus was used to load the osteon specimens and measure the elongations of the specimens (108). The elongation of the specimen under loading was measured by the change in resonance frequency of the apparatus' cavity. The accuracy in osteon specimen elongation measurements fell within 1%. The data determined that extinct specimens resisted tension better than alternate cylindrical specimens at both initial and final stages of calcification. The elastic modulus increased by at least 22% between initial and final degree of calcification. At final degree of calcification, the elastic modulus was found to be 114% larger for the extinct osteon than for the alternate osteon.

Tensional loading of single lamellae (Figure 5) was carried out in an experiment using material from femoral shafts. Investigators used alternate osteons at initial and final stages of calcification for the experiment. The specimens were cut into cylindrical shapes. The lamellae with collagen bundles that had a transverse spiral direction were then isolated using a procedure in which the specimen

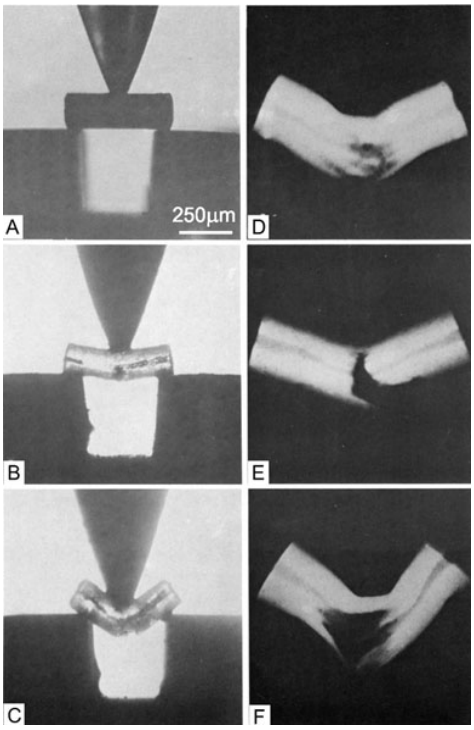

Figure 6. Three-point bending test. (a) A cylindrical osteon specimen is positioned for three-point bending. Testing of (b) alternate specimen and (c) extinct specimen. Micro-X-ray of (d) an alternate and (e) an extinct specimen. (f) Micro-X-ray of this alternate specimen shows an irregular fracture pattern. Reproduced with permission from ref #111.

was compressed perpendicularly to its axis and then pressured at changing diametral points. The isolated lamellae were cut longitudinally, then carefully straightened into ribbon-shaped specimens under microscope observation. The lamellae showed collagen following the direction parallel to the length of the ribbon-shape. The microwave extensometer used for monotonic tensional loading of osteons was adapted to measure the changes in length of lamellae under tensional loading along their ribbon-shape length. Since there was great variation in thickness within and among single lamellae, differences in ultimate tensile strength and modulus of elasticity between different degrees of calcification could not be computed. Ultimate load did not depend on the degree of calcification of the lamellar specimen (109).

5.4. Monotonic compression test

Extinct, alternate and bright osteons were investigated (17). Cylindrical specimens at both initial and final degrees of calcification were used for this experiment. The specimens had a height of 500 micron and the ratio of height to diameter varied between 2.5 and 3. There are two methods that can be used to load and determine the changes in specimen length due to compression. Both are accurate and, unlike tension methods, one of the compression methods permits the investigators to determine the osteon CPL type before isolating the specimen. A special device composed of a thin steel needle inserted into a dental drill was used to isolate the specimens. As the drill and the needle turned, the needle tip cut an osteon specimen with a cylindrical shape that had walls of uniform thickness.

The specimens were loaded by means of a micro-compressor with a microwave micrometer based on the cavity and pulse technique used to measure the tension resistance. The length change measurements were accurate up to 1%. Unlike tensional behavior, the elastic modulus and compressive strength values were maximum for bright osteons, intermediate for alternate osteons and minimum for extinct osteons at the same degree of calcification. These values increased as the osteons became more calcified. The elastic modulus increased by at least 29% between initial and final degree of calcification. At final degree of calcification, the elastic modulus was found to be 47% larger for the bright osteon than for the extinct osteon.

In the second compression test, the same osteon specimen shape as used for tension loading is used. The drawback in this method is that determining the osteon type can only occur after loading the specimens.

5.5. Pin-test

The pin-test measures the osteon wall resistance to internal pressure. Extinct, alternate and bright osteons were tested at both initial and final degrees of calcification (110). Cylindrical specimens were used for this experiment. The specimens had heights of 100 micron and diameters that ranged between 150 and 230 micron. Investigators measured osteonal cell wall resistance by gradually pushing a steel cone through the vascular canals until they fractured. The cone that gave the most precise results of osteonal cell wall resistance had an angular width of 35 degrees. In order to fracture the vascular canals, the investigators loaded the cone onto the specimen and gradually added weights onto the cone. The increasing weight on the cone caused it to progressively press down on the upper end of the vascular canal. The osteons deformed at first, and then the lamellae began to fracture. The lamellae that fractured first were the ones closest to the vascular canal.

The same microwave micrometer from previous techniques was used to measure the increasing drop of the cone until fracture. Bright osteon specimens were found to have the maximum final expanding strength, with alternate and extinct specimens having intermediate, and minimum strengths, respectively. This result gives further evidence that osteon wall resistance is increased by the presence of bright lamellae.

5.6. Bending test

Extinct and alternate osteons at the final degree of calcification were used for this experiment (111). Cylindrical specimens were prepared. The specimen height measured 500 micron. The specimen diameters measured 195 micron and the Haversian canal diameters ranged between 40 and 50 micron. The specimen was placed between two steel strips that were on the same horizontal plane so that its middle portion was not supported (Figure 6). Each end of the specimen had approximately 50 micron

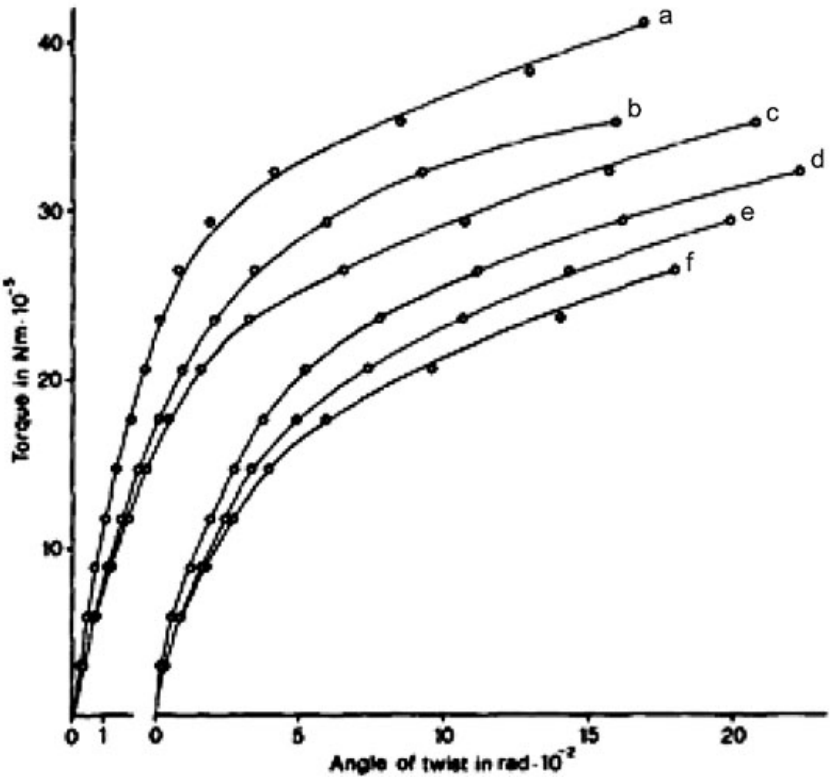

Figure 7. Monotonic torsion test. The graphs of (a-c) three extinct specimens show higher resistance to torsion than the graphs of (d-f) three alternate specimens are shown. Reproduced with permission from ref #19.

resting on the steel strip surface. Investigators loaded a steel point onto the unsupported center of each specimen. The steel point pushed down linearly on the specimen, causing it to bend at its center. The investigators used the same microwave micrometer used in early experiments. This gave an accuracy of the measurement of changes in bending within 1%.

Beam theory was used to calculate the ultimate bending load, ultimate bending deformation, elastic modulus and rupture modulus from experimental data, or these values were determined experimentally. The results concluded that extinct osteon specimens are not as resistant to bending as alternate osteon specimens. The alternate osteon specimens are more resistant due to their larger number of transverse bundles. Extinct osteons have few transverse collagen bundles, causing them to be less structurally compact than alternate osteons. At final degree of calcification, the elastic modulus was found to be at least 16% larger for the extinct osteon than for the alternate osteon.

5.7. Monotonic torsion test

Torsional loading of osteons has been tested with two different methods. Frasca *et al* (112, 113) created a method to test whole osteons, In the Frasca method, both single osteons and osteon groups were chosen without determining the type of osteon structural type or the degree of calcification. The specimens were tested wet and dry using a micro-torsional device. A laser light spot was reflected on a rotating mirror in order to evaluate the angular amplitudes. The investigators determined that strain and frequency rely upon shear storage modulus of both single osteons and osteon groups. Single osteons and osteon groups behave differently under torsion when they are wet and when they are dry.

While the previous method tested whole osteons, A. Ascenzi *et al* (19) developed a method to test osteon specimens. In the A. Ascenzi method, the investigators chose extinct and alternate osteons at final degrees of calcification. Cylindrical specimens connected to two lugs were used for this experiment. The osteon specimens had heights that ranged between 300 and 500 micron. The diameters of the specimens were 210 micron and the diameters of the Haversian canals were 40 micron. A special torsional device that was manufactured by the CECOM Company (Figure 7) was developed. The device consisted of a fixed axis and rotational axis, each axis complete with a set of jaws to secure the ends of the specimen. The specimens were attached to the fixed jaw on one end and the rotational jaw on the other. The rotational jaw turned and twisted the specimen as weights were added to it on the rotational axis. The specific weight that produced unchecked twisting of the specimen was the weight responsible for the failure of the osteons. The twisting angles of the specimen were measured using a laser beam reflection on a small mirror placed in the rotating jaws. They determined the ultimate torque, angular deflection, shear modulus, amount of energy absorbed up to

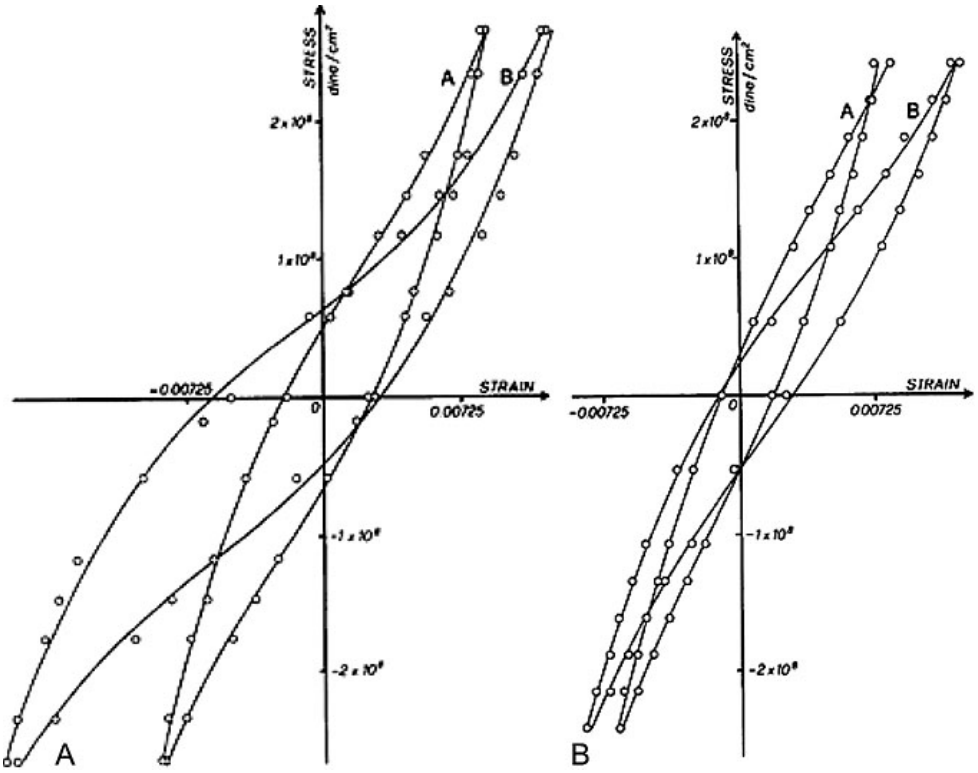

Figure 8. Cyclic tension-compression test. The diagrams of the first two full cycles of fully-calcified (a) extinct and (b) alternate osteon specimen show different mechanical behavior between the two specimens Reproduced with permission from ref #20.

failure and torsional shear stress either experimentally or by using the beam theory to compute it from experimental data. The results concluded that the extinct osteon specimens had higher ultimate torque and shear modulus values than alternate osteon specimens. The shear modulus was found to be 35% larger for the extinct osteon than for the alternate osteon.

5.8. Shear test

Extinct, alternate and bright osteons at both initial and final stages of calcification were tested on their shearing resistance using a double-shearing strength test (114). Cylindrical specimens were used. The specimens had heights of 300 micron and osteonal diameters of 200 to 300 micron. Femoral mid-shafts were cut into transverse sections with osteons oriented perpendicularly to the section plane. Each transverse section was placed on a flat surface with a hole cut from the center. This flat surface acted as a supporting plane for the specimen. The investigators placed a steel cylinder on top of the specimen, orienting it with the osteonal axis. The cylinder had a diameter smaller than the osteonal diameter and was called a "punch". The investigators slowly added weights to the punch, causing it to put pressure on the osteon. This pressure first caused the osteon specimen to deform and then the lamellar connections of lamellae surrounding the punch began to break. The ultimate shearing strength was determined when the connections between lamellae were broken and the osteon specimen began to fall through the hole in the supporting plane.

The same microwave micrometer from previous techniques was used to measure the advancing drop of the punch until reaching the concluding shearing strength. They determined that extinct osteons have the lowest resistance to shearing stress, suggesting that circular collagen bundles strengthen bone compactness of other osteon types. As the specimens' calcification increased, the strength and elastic modulus in shear increased. The elastic modulus increased by 2 to 22% between initial and final degree of calcification. At final degree of calcification, the elastic modulus was found to be 25% larger for the extinct osteon than for the alternate osteon.

5.9. Cyclic tension-compression

Because bone undergoes repetitive, or cyclic loading (e.g. femoral shaft during walking), the degeneration of the mechanical properties of single osteons under cyclic tension-compression was investigated in the 1980's (115). Extinct and alternate osteons at both initial and final stages of calcification were prepared as cylindrical shapes with lugs. The cylindrical part of the specimens had a height of 500 micron and a diameter between 166 and 284 micron. The microwave system previously described (section 5.1) was adapted to measure changes in sample length. One lug of the specimen was attached to the mobile part of the device and one lug was attached to the immobile part. The osteon specimens were subjected to loading-unloading cycles of 40sec. Movement of the device exerted traction or compression on the specimen. Tension caused the specimen to elongate, while compression caused the specimen to shorten. The hysteresis loops of the specimens were recorded. At fixed degree of calcification, extinct osteons displayed a greater increase in strain during compression than during tension, indicating that larger creep is present in extinct osteons under compression (Figure 8). In contrast, alternate osteons

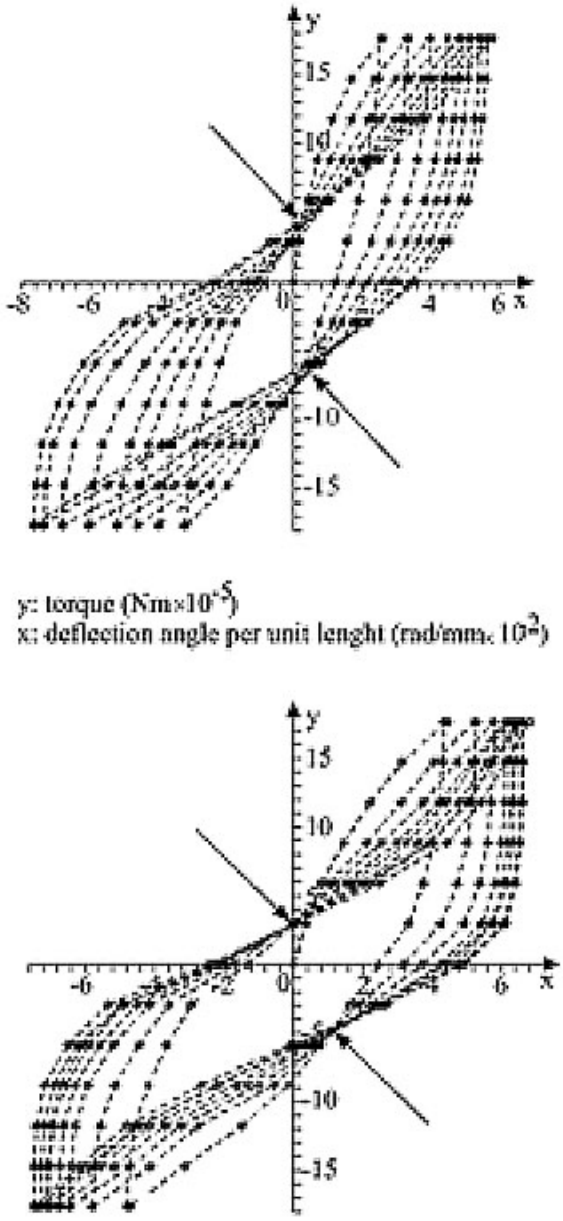

Figure 9. Cyclic torsion test. The diagrams of fully calcified osteon specimens indicate that the cyclic torsional behavior depends on percent of bright birefringence (a) 20% vs. (b) 54% by CPL. Arrows point to points of pinching. Reproduced with permission from ref #116.

showed a greater increase in strain during the tension when compared to compression, implying larger creep is present under tension.

When osteons are cyclically loaded, they display the degrading phenomenon known as pinching. Pinching is caused in osteons by injuries to their structure, such as flexural cracks or bond degradation. In a study in 1997, investigators studied cyclically loaded osteons (20). Similarly to a previous study in 1985, extinct and alternate osteon specimens in the shape of cylinders connected to two lugs were used for this experiment. The experimental osteons were at initial and final stages of calcification. Each specimen was subjected to cyclic tension-compression while the change in length was measured by the micro-wave instrument discussed in section 5.1. Results indicated that loading of the specimens involves mainly the longitudinal fibers of collagen. Lamellae with circular collagen bundles are prestressed and are not loaded along their axes. Therefore, extinct osteons with mainly longitudinal collagen/apatite bundles have more lesions causing pinching because they do not have circular bundles to protect them from collapsing when they are compressed and begin to deform. Alternate osteons have less longitudinal and more circular collagen bundles than extinct osteons; consequently they have fewer lesions that causing pinching. Increasing the number of cycles increased the strain limit and energy absorption and decreased the stiffness in both types of osteons due to the increasing magnitude of lesions and buckling. Extinct osteons had a greater strain limit in compression than tension in both the first and last cycles due to longitudinal collagen/apatite bundles protecting them more effectively when subjected to tension than when subjected to compression (16) Alternate osteons showed opposite results, having a greater strain limit in tension than compression due to circular collagen/apatite fibers preventing buckling and protecting them more effectively against compression than tension (17).

5.10. Cyclic torsion

This mechanical test was suggested by the present of pinching in the tension-compression hysteresis loops (section 5.9). The conjecture was that pinching was indicative of osteons' stability and resistance to micro-crack formation. If were the case, pinching would probably be present under a different cyclic-loading. Therefore, a different cyclic loading experiment was needed. It turned out that all osteon specimens tested under cyclic torsion showed pinching. Further, at the time the investigators determined to investigate osteons in terms of percent birefringent brightness by CPL that describe the range between the extinct and the bright osteons (Figure 1). Therefore, cylindrical specimens with lugs at final stages of calcification and increasing percent brightness by CPL were prepared (Figure 9; 116). The specimens had heights that ranged from 500 to 535 micron. The osteons' diameters ranged between 200 and 228 micron. The Haversian canal diameter measured about 40 micron. The osteon specimens were divided into groups in terms of range of dimensions. The micro-torsimeter previously used for monotonic torsion was adapted to allow both clockwise and counter-clockwise rotation. The lugs of the specimens were secured to the micro-torsimeter with the canal axis of each specimen aligned with the torsional axis. Starting with clockwise torsion orientation, the investigators engaged cyclic torsion by sequentially adding and and removing weights at a constant time of 4sec.

After the first half-cycle, all subsequent cycles on the diagrams share two points at which the cycles are pinched. Investigators examined how the stiffness and pinching of the osteon specimens degraded on the diagrams

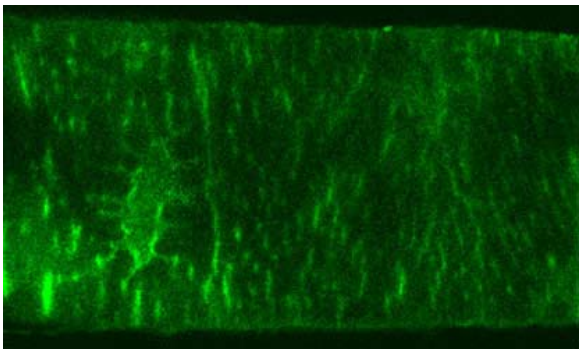

Figure 10. Osteocyte lacuna. Confocal microscopy allows for observation of osteocyte lacunae within the canalicular network. Canaliculae running longitudinally are visible on extinct lamellae. Reproduced with permission from ref #118.

of torque versus deflection-angle-per-unit-length as they increased the number of cycles. They looked at these cross-sections of specimens under CPL to compare them to the diagrams. In order to describe pinching, investigators adapted material science's Bauschinger effect. The Bauschinger effect was initially classified for metals, but later expanded to involve structures reinforced with metal bars. To explain pinching, investigators used material science's prying effect, the magnification of eccentric tensile load using levers. The mathematical fixed-point theorem was used to analyze the two points through which all full cycles pass. The hypothesis was the presence of a prying effect at the interface between the apatite crystallites and the non-calcified collagen fibril bands. As the percentage of collagen-apatite components forming a greater angle with the osteonal axis increases, the prying effect increases, and the number of micro-cracks increases more than their length as the number of cycles rises.

In conclusion, (1) the experiment helps differentiate characteristics that determine the micro-mechanical behavior in terms of collagen anisotropy by CPL and osteon size (44, 49); and (2) the occurrence of pinching helps explain the bonds between collagen fibrils and carbonated apatite crystallites.

6. ADDITIONAL MICROSCOPY TECHNIQUES

Magnification and resolution higher than those afforded by compound microscopy were needed to observe collagen and apatite patterns and interface between collagen and apatite as well as specifications of elementary components.

6.1. Confocal microscopy

Scanning confocal microscopy on isolated lamellar specimens is a method of assessing canalicular and collagen orientation patterns through lamellar thickness, which is the radial direction of the osteon prior to isolation (Figure 10). Confocal microscopes attain a higher magnification and resolution than compound microscopes and employ a pinhole opening in front of the photo-detector that allows observation at specific depth of specimen. In fact, a point-by-point brightening procedure prevents unfocused light coming from above and below the plane of focus from arriving at the photo-detector. This method allows observation of different collagen orientation patterns in successive planes of focus throughout the thickness of the specimen.

Extinct and bright lamellar specimens by CPL were examined by confocal microscopy (44, 117, 118). The arrangement of the collagen was measured using confocal microscopy image stacks. They determined the different collagen orientations using polarized light microscopy and the local collagen arrangement as it moved through the thickness of the specimen using X-ray diffraction. The investigators scanned the lamellar specimens when they were wet. It was not necessary to stain the specimen due to the natural fluorescence of the wet bone, also called endogenous fluorescence (119). Atoms and molecules absorb light at specific wavelengths and then emit that light at longer wavelengths than absorbed (120). The protein content of bone is dominated by collagen type I (119, 121), which has a fluorescent light range between 300 to 700nm (122). Therefore, confocal microscopy uses lasers of wavelengths within this range. Argon-ion lasers with wavelengths of 405, 514 and 594nm supplied equivalent images with the same quality in the fluorescent components. Because the other principal components of bone do not show fibrous patterns throughout lamellar specimens as collagen does, the auto-fluorescent images at 3000-4000x were concluded to be collagen. The extinct and bright outermost lamellae were isolated (Figure 4d). The isolated lamellar specimens measured between 5 and 15 micron in thickness. The specimens were first flattened and then inspected to ensure there were no cracks.

Collagen bundles are observed using confocal microscopy on the background of mucopolysaccharides and glycoproteins. Collagen fibers are dispersed in layers overlying each other through the thickness of the lamellae. The collagen bundles had mostly a unidirectional orientation and areas of these bundles are called domains (123). Domains gradually change throughout consecutive layers by a few degrees and several can be visible along down the length of the same layer in both types of lamellae. The direction of the fibers also changes within each layer. Confocal microscopy allows investigators to control their depth of field and separate the different collagen orientations that overlap as they move through the lamellar thickness, helping them to evaluate the different collagen orientation patterns (118).

In both extinct and bright specimens, collagen bundles that were cut during isolation of the lamellae appear as dots. These bundles are arranged almost perpendicular to the lamellae. The extinct and bright lamellae show different patterns of collagen arrangement in the confocal microscopy images. In the extinct lamellae specimens, the collagen bundles follow the specimen's breadth, illustrating parts that have a polished fibrillar structure. These fibrils for the most part have a 90 degree or smaller angle to the width of the specimen, while the bright lamellae collagen bundles have a roughly 45 degree angle

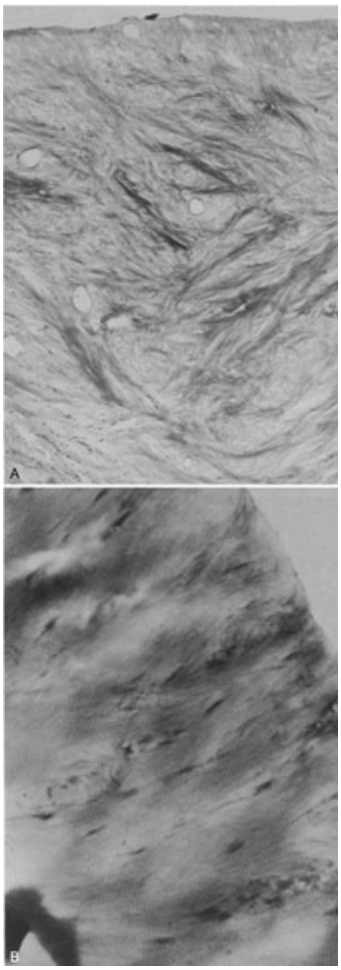

Figure 11. TEM of osteon specimens. Electron microscopy of ultrathin section shows (a) collagen oriented at approximately 45 and 135 degrees with respect to the longitudinal edge of the specimen at the boundary between two adjacent lamellae that appear respectively bright and extinct in transverse section (x12,000); (b) collagen fibrils orthogonal to the longitudinal edge of a lamellar specimen that appears bright in transverse section (x22,000). Reproduced with permission from ref #126.

to the width of the specimen. Extinct lamellar collagen bundles are also clearer in the more spread out areas than the bright lamellar bundles. In extinct lamellae, collagen arranged longitudinal to the osteon axis shows a parabolic distribution, while this distribution is seen in collagen oriented transverse to the osteon axis in bright lamellae. Collagen arranged oblique to the osteon axis in both types of lamellae also show a parabolic distribution through the thickness of the specimen. Both transverse collagen in bright lamellae and longitudinal collagen in extinct lamellae have their peaks at middle third of the thickness of the lamellae. In both extinct and bright lamellae, the oblique collagen peaks at the outer thirds. Extinct lamellar specimens display mostly longitudinal collagen arrangement and bright lamellar specimens typically have oblique collagen orientations to the osteon axis.

Collagen components seem to be less tightly packed when observing them under confocal microscopes than when observing them under high-resolution electron microscope. The electron microscopes give images that have a magnification at least five times higher than confocal microscopes. Confocal images are also enlarged two or three times, so the collagen orientation resolution is reduced due to a sharp change between dark and bright pixels. This shows a lack of information that would be provided by higher-resolution microscopes and causes collagen fibrils to seem less tight in confocal images. On one hand, CPL allows for observation of a larger area of focus than confocal microscopy, and therefore of variation of orientation of collagen on a wider region. On the other hand, confocal microscopy allows for observation of changes in collagen orientation within the depth of the specimen (117). Confocal microscopy was also used on bone section transverse to the shaft of the long bone (124). The results are discussed in section 8.

Confocal microscopy is a one-photon microscopy technique. Multi-photon microscopy allows for increased resolution especially in connection with second harmonic generation. Multi-photon microscopy has been applied to cancellous bone but not cortical bone (125).

6.2. Electron microscopy

Various types of electron microscopy have been applied to bone by many research groups around the world since the 1950's. The magnification of transmission electron microscopy (TEM) ranges up to 10,000,000x and up to 1,000,000x for scanning electron microscopy (SEM). In particular, both TEM and SEM have shown the orientation patterns of collagen fibrils within osteons. TEM showed patterns that were found in agreement with patterns established by other techniques. The collagen bundle orientation was observed to form criss-crosses, many at an angle of 45 degrees with respect to the edge of the bright lamella (Figure 11; 126).

For SEM observation, the bone specimens are examined after they are extracted with ethane diamine for two days and then rinsed in absolute ethanol, which removes the organic phase and leaves the mineralized phase. The mineralized phase follows the orientation pattern of collagen bundles no longer present in the specimen. The specimens are then observed by SEM to determine the mineralization and the different collagen bundle patterns (123). Before scanning, SEM specimens must first either be permanently mounted or coated. When mounted, the specimens are attached to a metal support that changes according to the type of SEM used. Sufficiently sturdy specimens can be scanned without metal support in the SEM (127). Bone specimens can only be analyzed without a conductive coating if they are scanned at a low accelerating voltage. For backscattered electron imaging, scientists use carbon coating. Gold, silver or gold-palladium coatings help increase the SEM signals (128). Removal of the coating material is used to remove the cells, matrix or embedding medium of the bone specimen. After properly preparing the specimens, the beam voltage and current, orientation of the specimen, signal mode and

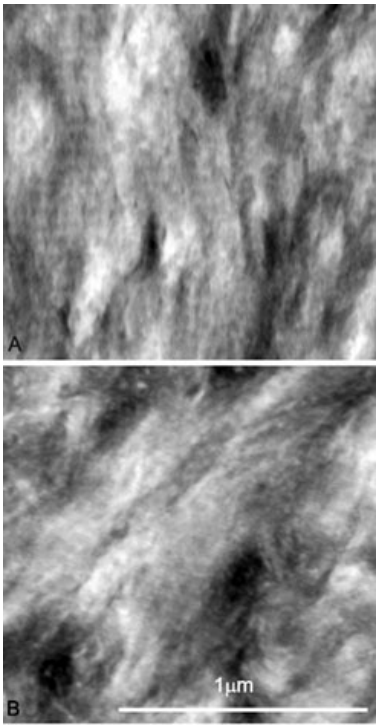

Figure 12. STEM of osteon specimens. STEM in TEM mode shows collagen orientation (a) along the longitudinal direction of lamella that appears extinct in transverse section; and (b) forming larger angles with the longitudinal direction of lamella that appears bright in transverse section.

detector strategy must be chosen in order properly to scan the specimen (127). The images of collagen bundles in extinct osteons have longitudinal and nearly longitudinal orientations, while the images of bright osteon collagen bundles show mostly coexisting longitudinal and transverse bundles (129). SEM demonstrates that canicular densities remain relatively constant throughout secondary osteons (66). SEM images also show the differences between normal and abnormal bone specimens. Normal bone shows ordered structure, while abnormal bone with overgrown organic tissue appears disordered (130). SEM has shown that collagen bundles run longitudinally in extinct osteons and both longitudinally and transversely in bright osteons (129, 131). SEM also indicates that extinct osteons are composed of thicker lamellae and contain more numerous osteocyte lacunae (131).

The scanning transmission electron microscope (STEM) can be used in either transmission or scanning mode. Recently, STEM in TEM mode was used to observe the sections with the width of the section, oriented parallel to the Haversian canal, as the reference direction for the orientation of collagen bundles. Specimens were prepared following the protocol for TEM as here set forth (126). Longitudinal bone sections were dehydrated and embedded in Araldite® (Huntsman Advanced Materials Americas Inc.). Ultra-thin 70-80nm serial sections were prepared with MT-1 Ultra Microtome (DuPont Instruments- Sorval, Miami, Florida) using a diamond cutter. The specimens were placed in TEM grids. Each grid containing the specimens was placed on a STEM holder and examined using a field emission gun scanning electron microscope (FESEM, Zeiss SUPRA VP-40) equipped with a STEM detector at an accelerating voltage of 20kV and at a working distance of 4mm. The STEM rasters the focused incident probe across the specimen that, as with the regular transmission electron microscope, has been thinned to facilitate detection of electrons scattered through the specimen. The STEM detector enables pure bright field, or extinct field, imaging to achieve optimum contrasts and rich imaging details of unstained thin sections. Further, the transmission mode of the FESEM has the advantages of avoiding chromatic aberration. This allows for a larger aperture to obtain higher transmission, signal to noise ratio, and contrast enhancement due to the lower electron energy within the 10 to 30kV range. Collagen was observed preferentially running longitudinally, that is parallel, to the Haversian canal on lamellae that appear bright in longitudinal sections and therefore corresponding to extinct appearance in transverse section under CPL (Figure 12). Collagen was observed to form larger angles with the longitudinal direction on lamellae that appear extinct in longitudinal sections and therefore corresponding to bright appearance in transverse section under CPL.

SEM in backscattered mode (123, 132, 133) measures degree of calcification and provides an alternative to the high-resolution micro-X-ray method. Backscattered electrons are higher energy electrons and backscattered electron imaging is preferentially used to examine mineralized bone matrix (128). Specimens are first scanned by the SEM beam. Then the analog output of the backscattered electron detector is translated using the detector's voltage levels into pixels with gray-level values. The gray-levels correspond to the degree of osteonal calcification (132). Backscattered SEM images have shown that the degree of osteonal calcification decreases from the Haversian canal to the cement line (133).

6.3. Micro-computed tomography

Since the late 1980's, micro computed tomography (microCT) has been extensively used to assess bone mineral density (BMD) on human and animal bone specimens (Figure 13; 135). The microCT provides a 3D evaluation, while the micro-X-ray provides a two-dimensional (2D) evaluation. The specimens that can be microCT'd are usually smaller in size than specimens that can be micro-X-rayed. The resolution of the microCT is not as high as the 1 micron of the micro-X-ray. In particular, the microCT cannot detect cement lines and therefore distinction of single osteons from interstitial bone. The microCT is nevertheless appropriate for studies of cortical porosity. Micro-CT provides the basis for finite element (FE) models of bone that are helpful in the understanding of the role of calcification in biomechanical setting, such as implant-cement-bone interface (section 9). While regular CT scan provides a lower resolution of bone tissue, it provides a basis for FE models of macroscopic bone to which the micro-FE models are now beginning to be linked (section 9)

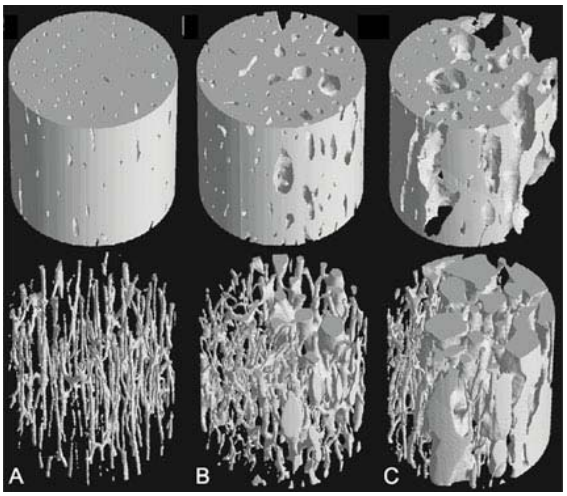

Figure 13. Micro-CT image of femoral mid-shaft. Micro-CT allows for automatic assessment of morphology in 3D. The top row depicts solid bone, while the lower row depicts porosity, of. (a) 20-year old female, (b) 61-year-old female, (c) 87-year-old female. Reproduced with permission from ref #134.

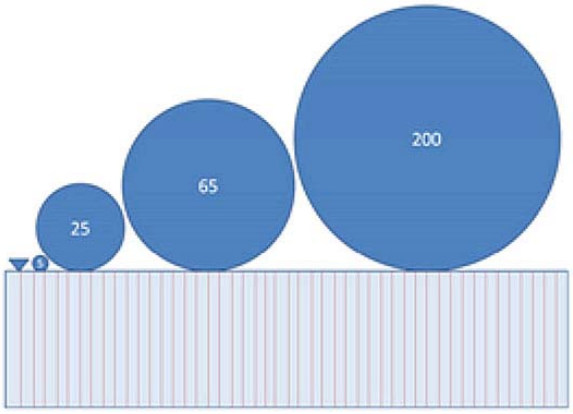

Figure 14. Nano-indentation. This schematic shows the variation of the contact between size of pyramidal and spherical tips and lamellar thickness that averages 6 to 9 micron. Reproduced with permission from ref #137.

7. ASSESSMENT OF TISSUE PROPERTIES: NANO-INDENTATION

Nano-indentation allows measurements of structural and mechanical properties of bone at the tissue-level *in situ*. That is, nano-indentation allows the assessment of the mechanical properties of the tissue that forms either single osteons or single lamellae. This technique addresses the mechanical properties at a level lower in the hierarchy of bone than the single osteon and single lamella level previously addressed in this chapter by mechanical testing as a unit. The elastic properties of bone tissue computed from nano-indentation data vary according to skeletal site, micro-structural specifications and individual characteristics such as age. Bone tissue with high turnover rates has lower mineralization and elastic properties. The results of nano-indentation suggest that heterogeneity affects fracture risk (136).

A small probe presses on a flat surface to indent at a submicron depth. The measured force and displacement of the probe can provide an estimate of the elastic, plastic and viscous properties of the specimen. To measure the indentation properties of bone specimens, Paietta *et al.* used an indentation tip in the shape of a sphere to press down on specimens of cortical bone (Figure 14; 137). The investigators used a range of indentation depths as well as a range of spherical tip sizes in order to determine different effects on the nano-mechanical properties. A ramp-and-hold method with a constant loading and unloading rate of mN/s was used to test the how the specimens' lamellar bone structures influence their nano-indentation properties. The investigators determined that using a small tip creates a more plastic response while a larger tip creates a more elastic response. In order to give a more accurate estimation of the modulus, it is best to indent the specimens to low depths to prevent stiffening. Measuring smaller volumes also gives better information on the specific structural features (136).

Nano-indentation properties were found to be highly dependent upon the bone's lamellar structure. The difference in elastic properties found between anatomical locations may involve turnover rate and osteon type (136). A higher turnover rate reduces the mean age of the osteons and therefore reduces mineralization. Different distributions of osteon types by CPL can also affect the results of the penetration of the indenting tip because of the relative change in orientation between collagen-apatite orientation and orientation of penetration (137). Interstitial bone was found to be consistently stiffer than osteonal bone (138). This difference was used to estimate, from relative volumes of osteonal and interstitial bone, differences in the elastic modulus of whole bone at different ages.

8. MICRO-STRUCTURAL ANISOTROPY

The study of the orientation and organization of collagen and apatite within single osteons and single lamellae has evolved in time. At first collagen/apatite was hypothesized to form helicoidal, almost longitudinal patterns in extinct osteons, transverse patterns in bright osteons, and alternating orientations forming 90 degree angles in alternate osteons. In time, the understanding of the osteon structure has become more sophisticated so as to include the variation of the pattern with each of extinct and bright lamella and the transition of the pattern between adjacent lamellae. As this line of research progressed, another question relative to organization was investigated. It dealt with the link between the micro- and macro-structure and whether the collagen/apatite orientation had a meaning at the macro-structural level. In particular, the question was whether such orientation is random or site-specific.

8.1. Collagen orientation patterns in single osteon

Collagen orientation plays a major role in the formation, elongation and arrest of micro-cracks (118).

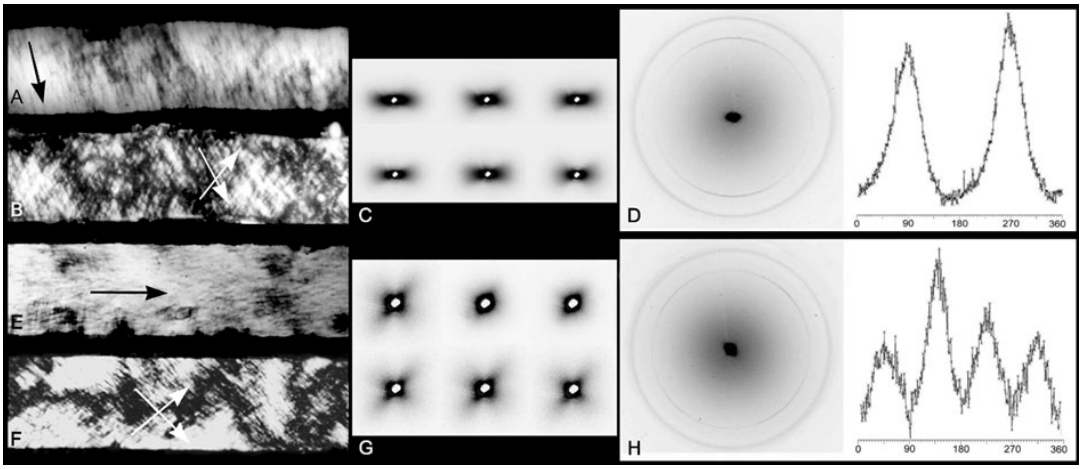

Figure 15. Collagen orientation patterns in single osteons. CPL image of lamella along the radial direction of the embedding osteon prior isolation shows collagen bundles' main orientation when the extinct lamella is rotated by (a) 45 degrees and (b) 0 degrees with respect to the polarizer. For the extinct lamella, (c) small-angle and (d) large-angle synchroton X-ray diffraction show dominance of collagen and apatite orientation along the original osteon axis. Collagen bundles' main orientation is shown when the bright lamella is rotated (e) 45 degrees and (f) 0 degrees with respect to the polarizer. For the bright lamella, (g) small angle and (h) large angle synchroton diffraction show dominance of collagen and apatite orientation at 45 and 135 degrees with respect to the original osteon axis. Reproduced with permission from ref #44.

Carbonated apatite crystals in osteons generally match the orientation of the adjacent collagen (38), which varies in the bone tissue, and can either facilitate or arrest the elongation of the micro-cracks that form at the collagen-apatite interface (139, 140, 141). Whether the lamellae outside the perilacunar region are extinct or whether they are bright, characterizes the orientation of the collagen in a cross section viewed under CPL (117). The extinct lamellae show a collagen orientation that generally forms small angles with the osteon axis, whereas the bright lamellae show a collagen orientation that forms larger angles (Figure 16). Collagen bundle orientation in the region around the lacunae is not random and follows specific patterns (Figure 17a, 17b). The collagen bundles and the adjacent canaliculi have a 360 degree distribution. For the lacunae in extinct lamellar specimens, 72% of observed collagen in the proximal, 72% of observed collagen in the distal, 81% of the observed collagen on the lateral left, and 79% of collagen at the lateral right, regions followed the adjacent canalicular orientation. For the lacunae in bright lamellar specimens, 72% of collagen in the proximal, 71% of the collagen in the distal region, and 80% of collagen in each of the lateral left and right regions followed the adjacent canalicular orientation. That is, for the mentioned percentages for each of the lamellar types, the collagen follows locally at the perilacunar region the canalicular orientation, which is circumambiently-perpendicular to the lacunar/ECM interface. The percentage of radially tilted lacunae with collagen following the adjacent canalicular orientation at the slender apex is significantly smaller in extinct, than in bright, lamellae.

Confocal microscopy was used to study collagen with its relation to caniculi and lacunae because it has a very high resolution when compared to polarized light microscopy and it allows investigators to directly monitor collagen orientation through consecutive images without gaps between slices. X-ray diffraction and electron microscopy were give collagen virtual slices with gaps between them, making them less preferable. Collagen orientation at the region around the lacunae that was away from the lacunar apices showed collagen orientation that mostly demonstrated circumambiently perpendicular orientation matching canalculi orientation in both extinct and bright lamellae types. Extinct lamellae appear to be thicker than the bright lamellae when looking at cross sections under CPL and confocal microscopy, implying that extinct lamellae would be able to have lacunae with larger radial tilts than bright lamellae would. It is more likely in collagen departing the perilacunar region that the extinct lamellae will show a smaller circumferential tilt than the bright lamellae (117).

The orientation of collagen and apatite affects micro-cracks' initiation and spread under axial loading (Figure 17c, 17d). Micro-cracks begin at the lacunar apices under axial loading, implying that they are associated with the osteocyte lacuna tilts in combination with the collagen and apatite organization. These fractures depend on the angle between the lacuna and osteon axes and on the surrounding tissue grain (140, 142). They will most likely form at the lacunar apex because extinct lamellae are more likely to have radially tilted lacunae than bright lamellae. Since the collagen is not as likely to orient itself with the canalculi at the apex in extinct lamellae, a micro-crack is less likely to radiate longitudinally, which helps reduce the chances of added propagation. However, in bright lamellae, micro-cracks are probably going to begin at the lacunar

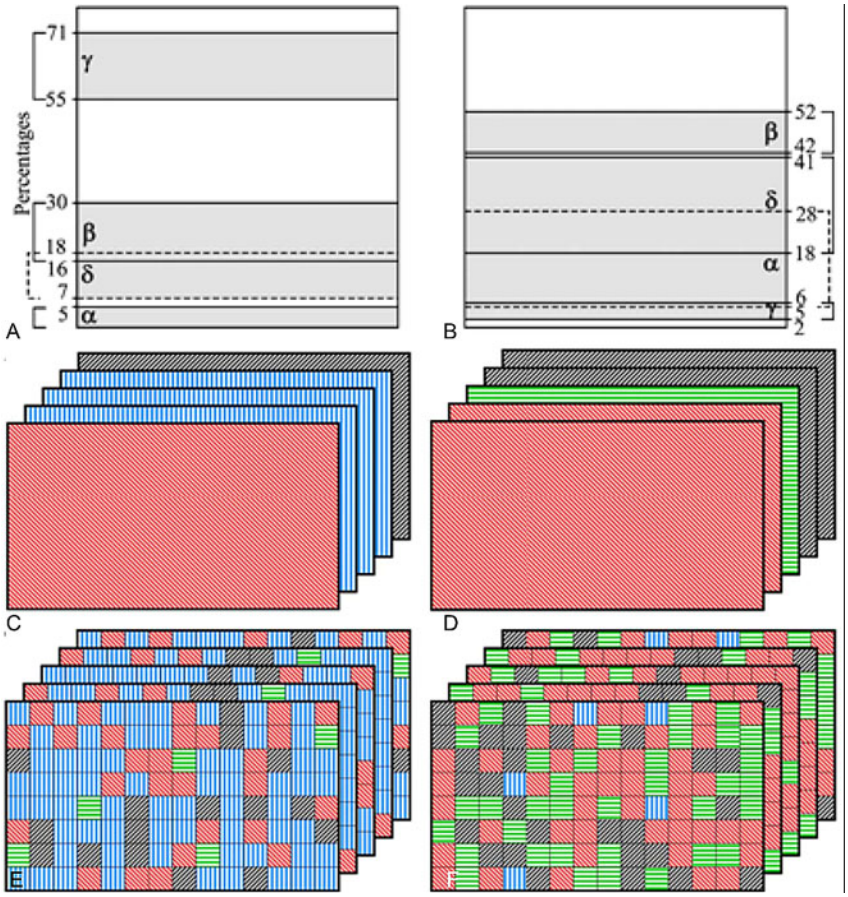

Figure 16. Quantification of collagen orientation patterns in single osteons. Percentages of collagen of (a) extinct and (b) bright lamella differ with respect to orientation that is generally transverse (alpha), oblique (beta and delta), parallel (gamma) to the longitudinal axis of the osteon. Because the distribution of collagen orientation was found to vary through lamellar thickness and circumferential length, the rotated plywood model for (c) extinct lamella and (d) bright lamella was updated to a more heterogeneous model, (e) and (f) respectively. Reproduced with permission from ref #32.

apex because the collagen does orient itself with the canaliculi and would turn away from the osteon axis. In bright lamellae, collagen bundles are oriented transversely to the axis (141).

8.2. Collagen orientation patterns in macroscopic bone

The distribution of collagen orientation within cortical bone is not random at load-bearing sites. Rather it forms 3D patterns in human bone, whether healthy or affected by metabolic disease, as well in animals (Figure 18; 21, 143, 144, 145, 146, 147, 148, 149). The patterns link collagen orientation to the force distribution during function. The percent of collagen forming small angles with the long bone axis is higher at the sites mostly stimulated in tension (e.g. tension due to bending of the femur) while the percent of collagen forming larger angles with the long bone axis is higher at the sites mostly stimulated in compression (e.g. compression due to bending of the femur). Additional research is needed to investigate how such distribution changes with age and with the presence of bone disease. For instance, when the macro-geometry of the bone is altered by rickets, the distribution of the collagen orientation is altered to compensate for the altered distribution of loading (21).

Collagen bundles are organized in 3D patterns in macroscopic bone through the specific osteon types classified by CPL (section 4.1). Such organization of osteons, perhaps in conjunction with their degree of calcification, may determine the bone tissue response to loading (145). In a study by Beraudi *et al.*, the three CPL osteon types were found differently distributed through the length of a human fibula. The alternate osteons dominated the mid-shaft, while extinct and bright osteons dominated proximal and distal ends of shaft. This differentiation may be linked to the force distribution at the fibula in terms of the combination of influence of collagen orientation within the lamellae on mechanical properties of osteons (section 5), adequate resistance of alternate osteons under both tension and compression than extinct or bright alone, and rarity of bright osteons (147).

9. MODELS AND SIMULATIONS

Hand-in-hand with the generation of experimental findings, mathematical and engineering techniques have been applied to carry out in depth data analysis. Models of secondary osteons and lamellae have been developed to reflect their multi-directional structures

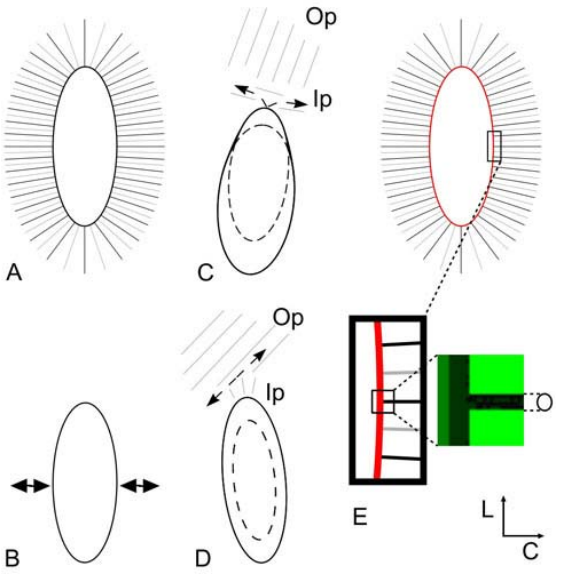

Figure 17. Micro-cracks in osteons. (a) Model of how collagen (lighter grey) is distributed with respect to canaliculae (darker grey) at the perilacunar region of osteocyte lacunae. (b) Both under tension and compression, the generally circumambiently-perpendicular orientation of collagen-apatite at the perilacunar region, parallels the direction of the greatest deformation at the equatorial region. (c) In the extinct lamella, the higher chance that the lacuna is tilted radially (depicted by the eccentric ellipses) and the lesser likelihood that the collagen follows the canaliculi at the apex, may facilitate deflection of a micro-crack. (d) In the bright lamella, a micro-crack would be deflected because of the high percentages of collagen-apatite orientation forming a wide angle (plus or minus 45º) with the axial direction. (e) The effect of the canalicular presence is stronger at the interface with the lacuna and maximum (in red) at the radial mid-lacuna equator (in square). The detail in the square is enlarged and rotated to show the canalicular section. Reproduced with permission from ref #118.

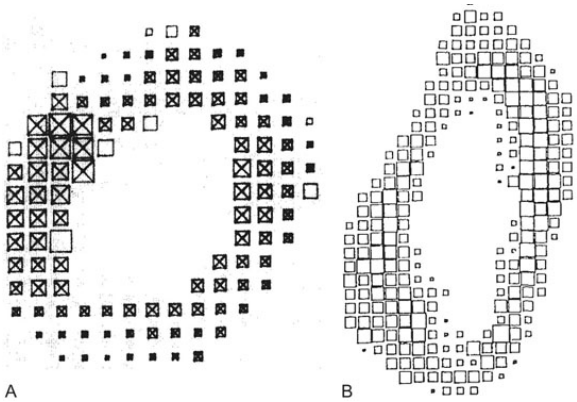

Figure 18. Collagen orientation patterns in macroscopic cortical bone. The percentage of bright lamellae were assessed at femoral mid-shaft of (a) young adult donor and of (b) donor whose femurs were deformed by rickets. The size of a square at a given location is proportional to the percent of bright lamellae within the field of focus centered at the location. The percent of bright lamellae vary through the cortical bone and differ between the normal femur and the femur whose curvature was affected by rickets. Reproduced with permission from refs #18, 143.

so as to investigate the functions of the elementary components when they are under different loading conditions (7, 110, 150, 151, 152, 153, 154, 155, 156, 157, 158, 159, 160, 161, 162, 163, 164, 165, 166, 167).

Over the years, 2D and 3D models of specific aspects of the Haversian system have contributed to the understanding of the experimental observation. A 2D model of the quarter-staggered configuration of collagen demonstrated the relationship of loci on individual collagen molecules within the fibril. For example, the amino-terminal edge of the "hole zone" is the site where the collagen molecule is cleaved by tadpole collagenase, by a disaccharide unit is covalently bound to the α1-CB5 peptide, and by the carboxyl-terminal intermolecular cross-linking. The carboxyl-terminal edge of the "hole zone" is the site of aminoterminal cross-linking (168). Material properties that depend on collagen bundle orientation and degree of calcification were included in the "lacuna-enhanced osteon" model, which is the first to include the collagen-apatite orientation of bone. This model investigated the influence of the collagen-apatite's orientation with respect to the loading direction in terms of the specimen's strain and stress fields. The model showed the axial deformation in the experiments and the difference in the greatest principal strain of the specimens (Figure 19; 16, 17, 20, 115).

The lacunar major axis parallels the axis of the osteons, and the model simulations of osteon with lacunae show that the lacunar strain concentration role (169, 170). The average concentration factor is the ratio between stress at the perilacunar region and axial strain on the osteon. The extinct osteons had higher average concentration factors than the bright osteons when observing them under elastic compression. Local mechanical response is not affected by larger perilacunar regions (171). The mid-equatorial region is the furthest region from the lacunar axis, so it moves the most as lacunar space decreases under tension and increases under compression. This causes it to have the greatest strains when it is stressed or compressed. Collagen orientation in this region can help the ECM to resist stress from tensional loading. The lacuna-enhanced model parallels the 2D osteon model with lacunae (172) and 3D "boxed" models of a perilacunar region of one lacuna and ten canaliculi (171). These three models show that perilacunar strains are intensified under tension and compression. The lacuna-enhanced osteon model simulation of canalculi with diameters of 1mm showed that canaliculi increase the strain at the equator of the lacunar wall (118).

In recent years, system biologists, mechanical and software engineers and applied mathematicians have increasingly collaborated towards developing 3D multi-scale virtual rendering of bone tissue able to address specific clinical issues (165, 166). On the basis of

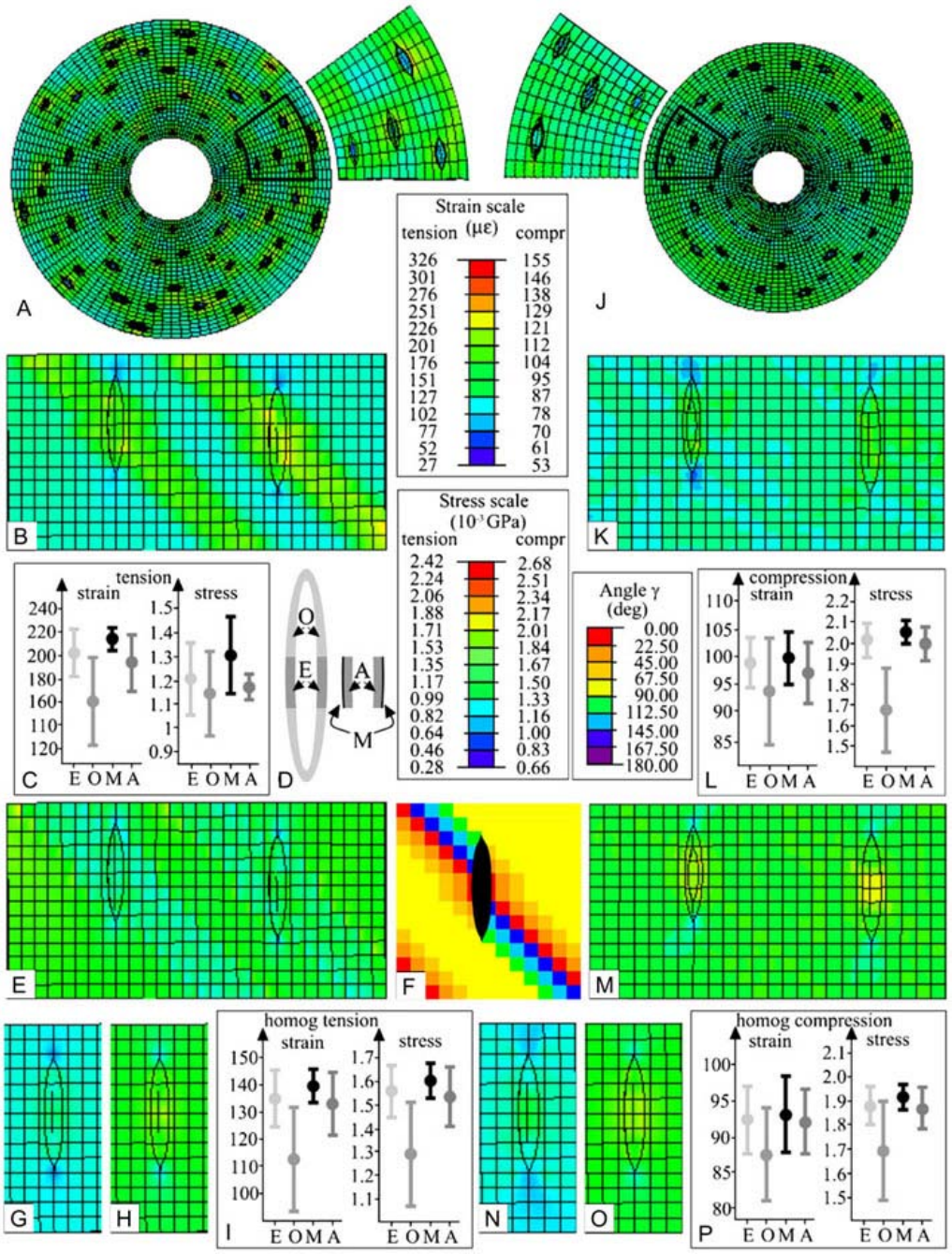

Figure 19. Simulation of monotonic tension and compression test of single osteon. This series of images shows strain and stress distributions on a modeled osteon containing lacunae under either tension (a through i) or compression (j through p) along the osteon axis under the same load (10gr) within the elastic range. Meshing represents finite elements. (a) Under tension, maximum principal strains are shown on a complete transverse section with an enlarged detail and (b) a hemi-longitudinal section containing two lacunar sections. (c) This diagram show the mean (dot) and standard deviation (bar) of strain and Mises stress fields in the perilacunar region (d): (E) equatorial, (O) outside equatorial, (M) mid-equatorial, and (A), away from M in E. The distribution of Mises stresses relative to (b) is shown in (e). (f) This diagram shows the local collagen orientation on a detail of undeformed longitudinal section relative to (b) and (c). (g) Lower strains and (h) higher stresses are present in the homogeneous model than in the composite model (compare (i) with (c)). (j) Under compression, maximum principal strains are shown on a complete transverse section with an enlarged detail and (k) a detail of a longitudinal hemi-section containing two lacunae. (l) Mean (dot) and standard deviation (bar) for strain and stress fields under compression in perilacunar region (d). The distribution of Mises stresses relative to (k) is shown in (m). (n) Lower strains and (o) lower stresses are present in the homogeneous model than in the composite model (compare (p) with (l)). Reproduced with permission from ref #118.

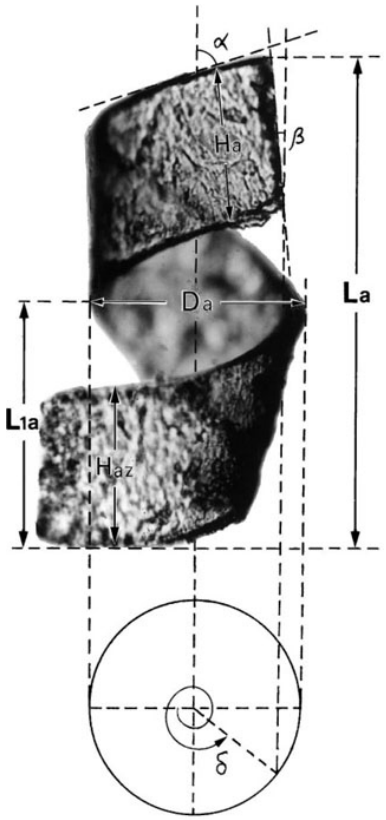

Figure 20. Model of prestress in single lamella. On the bright lamellar specimen isolated and slit axially, La denotes the outer linear length; L1a the outer linear length corresponding to one revolution; Da the outer diameter, Ha the outer height and Haz the outer component of the height along the helicoidal axis, alpha the angle of inclination with respect to the helicoidal axis, beta the angle of inclination of the two edges created by the axial slit with respect to the helicoidal axis. The angle delta, which measures the extent of specimen wrapping along its axis, was measured directly on the specimen. The linear length La is the distance along the helicoidal axis between highest and lowest extremity. The linear length L1a corresponding to one complete revolution is the distance on helicoidal axis between two consecutive threads of the helicoidal shape. Reproduced with permission from ref #15.

definition by clinicians of the challenges that they face, expert researchers in disparate fields, from orthopaedics, dentistry, bone biology, biomechanical engineering, and biomaterials, to applied mathematics are pushing the limit of their individual expertise to share techniques specific to each field, that, appropriately marshaled, make possible to prepare and validate cost-effective hierarchical (or multi-scale) models for clinical assessment of bone. The clinical problems that are viewed from a multi-scale perspective are: (i) assessment from bone parameters of bone fracture risk at various skeletal sites, including hip and spine, (ii) evaluation of osteo-integration of implants at hip, knee, spine, mandible and maxilla; (iii) evaluation of stress adaptive bone remodeling and bone repair in the presence of disease at various skeletal sites including hip, knee, spine, mandible and maxilla, and (iv) appraisal of effect of bone metastases on the mechanical properties of the bone tissue. In the US, the Interagency Modeling and Analysis Group aims and the National Institutes of Health Roadmap have encouraged researchers to design a common plan of action to develop state-of-the-art 3D multi-scale models of bone. Experts from different fields will likely continue to need to teach each other the latest developments concerning bone modeling and to design collaborative plans to solve challenging problems.

In the last two decades, clinicians have used imaging to assess bone quality, broadly understood as the ability of the bone tissue to perform its appropriate function. Dual energy X-ray absorptiometry (DXA), quantitative ultrasound, quantitative computed tomography, peripheral quantitative tomography, microCT, magnetic resonance, radiographic texture analysis, and FE models based on such imaging methods, have shown that BMD, trabecular and cortical micro-architecture, mass, and tissue mechanical and compositional properties, play an important, but yet undefined role in bone quality. Such parameters are in turn varied as functions of age, sex, weight, height, previous fracture occurrence, parent hip fracture, smoking, use of glucocorticoids, rheumatoid arthritis, secondary osteoporosis, and alcohol consumption (173). Since 2000, when the scientific community reached the conclusion that BMD alone does not assess the biomechanical health of the bone tissue, the interest in bone micro-structure has mounted. However, the imaging techniques mentioned and the related modeling do not view the bone tissue below a resolution of 0.5mm. At such resolution, the micro-structural elementary components are indiscernible.

From a bio-material point of view, bone can be considered a natural composite-hybrid material (174) in terms of the three-phases of (i) organic collagen fibers, (ii) inorganic carbonated hydroxyapatite crystals and (iii) a matrix of additional proteins and water (section 3). Both the collagen-apatite orientation and the degree of tissue calcification were found to vary through the tissue and play a role in the local material properties of the bone tissue (sections 4 and 5). For instance, collagen-apatite orientation and the degree of tissue calcification affect the osteo-integration at the bone-implant interface (141). By creating discontinuities in the bone tissue, osteocyte lacunae were found to alter the strain and stress distribution at the perilacunar region (118, 170). Both collagen-apatite orientation and presence of osteocyte lacunae are hypothesized to play a role in the elongation, propagation and arrest of micro-cracks (141). The mechanical stimulation of the osteocyte lacuna is of great interest to researchers in reference to the potential role of the osteocyte in mechano-transduction (167). The cited literature shows that laboratories around the world have amassed significant information on the biomechanical implications of micro- and nano-structures. There is accordingly a sufficient knowledge about the lower level structures to undertake the challenge of interfacing the various multi-scale levels in integrated models.

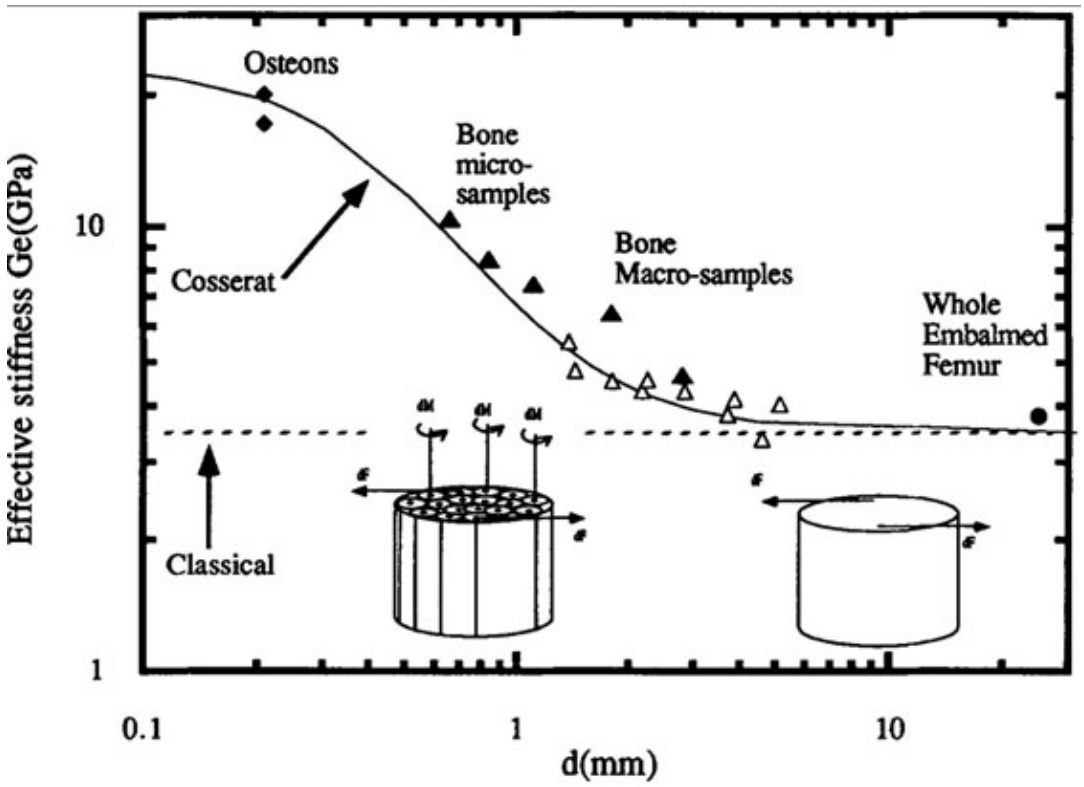

Figure 21. Reconciliation of macro- micro- material properties. The diagram illustrates the variation of mechanical properties across the multiple scales of bone structure. Reproduced with permission from ref #184.

Systemic modeling and simulation approaches for multi-scale structures have greatly developed during the last decade. Currently, extensive research is devoted to the linkage of the material and mechanical properties of cortical bone among the various levels of the hierarchy (175, 176). The study of the mechanical properties of macro-specimens per se has been matter of research by many investigators (e.g. 177, 178, 179, 180, 181, 182, 183). The question of the ultra- and micro-structural specifications that lead to macroscopic fracture remains largely unknown. Micro-structural heterogeneity is hypothesized to have direct bearing upon the fracture behavior of the Haversian cortical bone because the micro-crack behavior varies in dependence of the specifications of the elementary components that form the micro-structure. A mathematical structural model of prestress in the bright lamella allows estimate of the magnitude of the prestress and proposes a role of the oblique collagen bundle of the bright lamella in the prestress mechanism (Figure 20; 15). Other phenomena are present at the micro-structural levels that cannot be observed in macroscopic specimens because they become buried in the complex variation of tissue level parameters within the macro-specimen. For instance, pinching of osteons' hysteresis loops is characteristic of the micro-structure (sections 5.9 and 5.10). Application of the fixed-point-theorem allowed interpretation of pinching in terms of high stability of osteon structure and resistance to micro-cracking (116). Engineering theories, such as Cosserat theory, continue to be applied to reconcile the parametric changes of bone mechanical properties across the hierarchical levels to understand the contribution of each structural scale to the overall behavior of bone (Figure 21; 184).

The loading conditions and the specifications of the Haversian system each guide the direction of micro-crack growth. Short cracks are found more frequently in tissue than long cracks. Under tension, osteons have been observed to act as stoppers of micro-cracks coalescing and propagating through the interstitial bone. However, if a micro-crack elongates to a critical length, the micro-crack can penetrate osteons and then move through the lamellae in the osteon. If the micro-crack is able to break through a Haversian canal, the bone will likely fracture. If osteons are loaded under compression in the same direction as their micro-cracks, it is likely that the micro-crack will enter the osteon (185).

Traditional mono-scale approaches have been found inadequate to model multi-scale materials because of the range of scales and the prohibitively large number of variables involved (186). Because the multi-scale environment often shows that different scales are governed by characteristically different physical laws (e.g. quantum mechanics at one scale and classical mechanics at another), fields such as mathematical physics and stochastic processes are developing rapidly (187, 188). Approaches such as the Car-Parrinello method, quasi-continuum method, super-parametrization, heterogeneous multi-scale method, Vanden-Eijinden's method, coarse-grained Monte-Carlo models, adaptive model refinement and patch dynamics, have become available for possible bone

applications.

Homogenization theory allows computation of the material properties of one scale from the components of the sub-scale. It has been applied to FE models of groups of secondary osteons (e.g. 157). Various homogenization approaches are now being adapted to evaluate properties effecting bone tissues: (1) numerical up-scaling to compute effective mechanical properties; (2) asymptotic expansions based on multiple scales to derive effective parameters as functions of solution on the lowest scale; (3) analytical relations based on spectral representation, which give the effective property of bone tissues as an analytic function in the complex plane; and (4) coupled bounds to evaluate bone tissue properties from other known parameters (e.g. estimation of permeability or elastic moduli from electric properties). Mathematically challenging problems are related to the computation of viscoelastic properties: e.g. nonlinear dispersive models of bone marrow and nonlinear homogenization methods. Homogenization can also be adapted to assess bone structural properties from acoustic and electro-magnetic waves in bone tissue (e.g. 169).

Often defined as the "science of patterns" (189), mathematics can be applied to identify statistical patterns within the variation of specifications of components (190). Also, the appraisal of the key micro-structural elements that vary statistically was investigated a decade ago by two distinct approaches. Yeong and Torquato (191) thoughts were in terms of pixel-by-pixel representations (conceivable by materials scientists), while Portilla and Simoncelli (192) use a wavelet basis (conceivable by image processors). This advancement in imaging analysis could be used to complement the current microCT studies that usually refer to relatively smaller regions. Indeed, the description of micro-structural variation in 3D throughout specific extended sites is challenging. Inverse problem approaches have started to be used to study the trabecular network, although not the Haversian network (193). Computational geometry also offers a variety of techniques for optimization of data collections from images (e.g. 194). Percolation theory, recently applied to ice to explain the global warming-induced process of ice melt (195) and to trabecular bone (196), can be applied to compact bone hierarchy and offers the potential to explain the porosity of one scale that can be compatible with the phenomena at the next scale.

Various groups around the world have built models of bone tissue that address portions of the bone hierarchy described by subsets of parameters. Such models are of: (1) a cell network within the mineralized matrix viewed as a combination of collagen and apatite needles; and (2) compact bone micro-structure comprised of single osteons or osteon groups characterized by various arrangements of elementary components. The removal of one of the limiting assumptions of isotropy becomes an engineering challenge with the introduction of the anisotropy. An example is the issue of which failure criterion to choose (197). Various publications of the last three years on bone tissue point to the need to combine the models that address two scales into a full 3D model that maintains the essential characteristics of each level (e.g. 198, 199). In addition to the insights from studies of the 3D multi-scale structure of bone to be gained in respect of the clinical problems here addressed, such studies will offer further insights pertinent to (I) the *in vitro* development of bioengineered bone and (II) the understanding of bone as an organ in the human body (200, 201, 202, 203, 204).

10. OPEN PROBLEMS

We consider here open problems from an experimental and a computational/modeling point of view. In terms of experimental/structural understanding of the relation between bone micro- and macro- structure, we have seen in the previous sections that the distribution of osteonic lamellae and interstitial bone in cross sections of long bone shafts is not random. In fact, the distribution of osteonic lamellae in cross sections of long bone shafts shows a pattern compatible with the shaft shape and the distribution of forces usually operating on long bone under both normal and pathological condition. In general terms, there is indication of a high incidence of birefringent extinct in bone regions loaded in tension and bright lamellae in bone sectors loaded in compression. Patterns should be defined under healthy and pathological conditions in relation to mechanical loading. Pending questions are (a) the relation between osteonic lamellar distribution and geometry of the bone shaft loaded in bending and torsion, with respect to the mechanical properties of extinct and bright lamellae; (b) the relation between osteonic lamellar distribution and geometry of the bone shape in determining fractures, especially in bending, with respect to the mechanical properties of extinct and bright lamellae; and (c) the structural classification of osteons in diaphysis of vertebrates, whose lamellar structure somewhat differs from that of humans, to increase accuracy of interpretations.

The effect of specific clinical factors on bone architecture that renders it prone to fracture is largely an open question. While age is known to decrease cortical porosity, the occurrence of fracture may be related to the distribution of the increased porosity and to the decreased heterogeneity of the tissue (205, 206). Interestingly, the mechanical properties of single osteon at specific degree of calcification do not change with age (16). Therefore, the weakening of bone may result from higher percent of older bone showing higher percent of osteons at late stages of calcification, higher percent of resorption lacunae, possibly altered collagen orientation and increased percent of micro-cracks. Such weakening may result in a fracture when it occurs at sites more mechanically challenged. Since the early 2000s the clinical community has reported occurrence of fractures not typical before use of bisphosphonates (207). So-called atypical femoral fractures usually occur without a fall in patients with increased femoral cortical thickness, just below the smaller trochanter or at mid-diaphysis, oriented transversely rather than spirally with a medial spike. Some of these patients had been on long-term bisphosphonate therapy.

The effect of anti-resorption bisphosphonates on

the micro-structural components of the compact bone is largely unknown. Bisphosphonates have been shown to lower the amount of bone turnover. Therefore, bone treated with bisphosphonates shows reduced bone loss and higher percentage of older tissue, i.e. more mature mineral and matrix bone tissue (208). Specifically, risedronate has been shown to curtail bone remodeling and lessen the area and number of cortical pores. Reduction of bone remodeling and porosity has been associated with reduced fracture risk in epidemiological studies (209).

The effect of bone anabolic agents on bone micro-structure is beginning to be explored. The effect of recombinant human parathyroid hormone PTH(1-34) has been investigated on patients affected by osteoporosis since the 1970's (210, 211, 212, 213, 214, 215, 216, 217). PTH(1-34) helps to build up bone regardless of whether it is given to patients alone or if it is given along with anti-resorptive treatments like estrogen and calcitonin. Short-term PTH(1-34) treatment has been associated with decreased fracture risk in patients (214, 218, 219) and animal models (220, 221). Male and female patients display different anabolic actions of PTH when studying their compact and cancellous elements. In post-menopausal women, cortical volume, cortical thickness, endocortical wall width and porosity increased notably (222). Studies that were focused to uncover the cellular or molecular means that lead to PTH's anabolic effect on bone have shown that PTH increases the mesenchymal stem cell number and activates the vascular endothelial growth factor (223). PTH treatment was also found to reduce osteocytic sclerostin and Dkk1, which negatively affect Wnt binding to Lrp5 (179, 180, 224, 225). Reduction of sclerostin by PTH would stimulate Wnt and Bmp, both of which stimulate osteoblast function (226, 227). In a recent study on the micro-structural component of iliac crest biopsies of post-menopausal patients affected by osteoporosis and treated with PTH(1-34), lamellar thickness was found to be increased in comparison to age- and sex- matched osteoporotic patients to match the thickness values of pre-menopausal women (228). If this result is confirmed at weight-bearing sites, the lamellar thickening by PTH(1-34) treatment may reverse the thinning of bright lamellae observed at the femoral neck of patients who suffered femoral neck fracture, but not present in non-fractured controls (229).

11. ACKNOWLEDGEMENTS

Maria-Grazia Ascenzi provided overall outline, references, writing and editing. Allison Roe searched references and contributed writing and editing.

12. REFERENCES

1. H. Petersen: Die Organe des Skeletsystems. In: Handbuch der mikroskopischen Anatomie des Menschen. Springer, Berlin (1930)

2. Galileo Galilei: Discorsi E Dimostrazioni Matematiche Intorno À Due Nuoue Scienze Attenenti Alla Mecanica & I Mouimenti Locali. Elzevir, Leiden (1638) (available at http://galileo.imss.firenze.it).

3. Francis Gaynor Evans: Mechanical Properties of Bone. Charles C Thomas, Springfield, IL (1973)

4. Antonie van Leeuwenhoek: An extract of a letter from Mr. Anth. Van. Leeuwenhoek, containing several observations on the texture of the bones of animals compared with that of wood: on the bark of trees: on the scales found on the cuticula, etc. Philos Trans R Soc London 202, 838-843 (1693)

5. Victor von Ebner: Ueber den feineren Bau der Knochensubstanz. S B Akad Wiss Wein 72, 49-138 (1875)

6. Louis Ranvier: Traité Technique d'Histologie. F Savy, Paris (1887)

7. W. Gebhardt: Ueber funktionell wichtige Anordnungsweisen der feineren und gröberen Bauelemente des Wirbeltierknochens: II. Speizeller Teil. Der Bau der Haverssohen Lamellensysteme und seine funktionelle Bedeutung. Arch Entwickl Mech Org 20, 187-322 (1905)

8. F. Weindenreich: Das Knochengewebe. In: Handbuch der mikroskopischen Anatomie des Menschen. Springer, Berlin (1930)

9. Rodolfo Amprino: Reported in G. Levi: Istologia, third ed. Unione Tipografico Editrice Torinese, Turin (1946)

10. R. Frank, P. Frank, M. Klein, R. Fontaine: L'os compact humain normal au microscope électronique. Arch Anat Microsc Path 44, 191-206 (1955)

11. R. Frank: Contributions á l'étude au microscope électronique des tissues calcifiés normaux et pathologiques. Thèse de Doctorat en Médecine. Strasbourg, France (1957)

12. J. W. Smith: The arrangement of collagen bundles in human secondary osteons. J Bone Joint Surg 42B, 588-605 (1960)

13. Stephen A. Reid: A study of lamellar organization in juvenile and adult human bone. Anat Embryol 174, 329-338 (1986)

14. Marie-Madeleine Giraud-Guille: Twisted plywood architecture of collagen fibrils in human compact bone osteons. Calcif Tissue Int 42, 167-180 (1988)

15. Maria-Grazia Ascenzi: A first estimation of prestress in so-called circularly fibered osteonic lamellae. J Biomech 32, 935-942 (1999)

16. Antonio Ascenzi, Ermanno Bonucci: The tensile properties of single osteon. Anat Rec 58, 375-386 (1967)

17. Antonio Ascenzi, Ermanno Bonucci: The compressive properties of single osteon. Anat Rec 61, 377-392 (1968)

18. Antonio Ascenzi, S. Improta, Michele Portigliatti-

Barbos, S. Carando, Alan Boyde: Distribution of lamellae in human femoral shafts deformed by bending with inferences on mechanical properties. Bone 8, 319-325 (1987)

19. Antonio Ascenzi, Paolo Baschieri, Alessandro Benvenuti: The torsional properties of single selected osteons. J Biomech 27, 875-884 (1994)

20. Antonio Ascenzi, Maria-Grazia Ascenzi, Antonio Benvenuti and Francesco Mango: Pinching in longitudinal and alternate osteons during cyclic loading. J Biomech 30, 689-695 (1997)

21. Antonio Ascenzi: The micromechanics versus the macromechanics of cortical bone - a comprehensive presentation. J Biomech Eng 110, 357-363 (1988)

22. Rudolph Albert von Kölliker: Manual of Man Microscopical Anatomy. Lippincott, Grambo and Co., Philadelphia (1854)

23. D. Ziegler: Studien über die feinere Struktur des Röhrenknochens und dessen Polarization. Dtsch Z Chir 85, 248-262 (1908)

24. Elbert B. Ruth: Bone studies. I. Fibrillar structure of adult human bone. Am J Anat 80, 35-53 (1947)

25. C. -H. Rouillier, L. Huber, E. -D. Kellenberger, E. Rutishauser: La structure lamellaire de l'ostéone. Acta Anat 14, 9-22 (1952)

26. Arne Engström, Bengt Engfeldt: Lamellar structure of osteons demonstrated by microradiography. Experientia 9, 19 (1953)

27. C. -H. Rouillier: Collagen fibers of connective tissue. In: The Biochemistry and Physiology of Bone. Ed: Bourne G H, Academic Press, London (1956)

28. J. Vincent: Corrélation entre la microradiographie et l'image en lumière polarisée de l'os secondaire. Exp Cell Res 13, 422-424 (1957)

29. Gastone Marotti, M. A. Muglia: A scanning electron microscope study of human bone lamellae. Proposal for a new model of collagen lamellar organization. Arch Ital Anat Embryol 93, 163-175 (1988)

30. Gastone Marotti: The structure of bone tissues and the cellular control of their deposition. Arch Ital Anat Embryol 101, 25-79 (1996)

31. Susan Pfeiffer, Christian Crowder, Lesley Harrington, Michael Brown: Secondary osteon and Haversian canal dimensions as behavioral indicators. Amer J Phys 131, 460-468 (2006)

32. Maria-Grazia Ascenzi, Alexandre Lomovtsev: Collagen orientation patterns in human secondary osteons, quantified in the radial direction by confocal microscopy. J Struct Biol 153, 14-30 (2006)

33. Maria-Grazia Ascenzi, Marta Andreuzzi, John Michael Kabo: Mathematical modeling of human seconday osteons. Scanning 26, 25-35 (2004)

34. M. van der Rest: The collagens of bone. In: Bone. Vol. 3: Bone matrix and bone specific products. Ed: Hall B K, CRC Press, Boca Raton (1991)

35. David Eyre: Collagen of articular cartilage. Arthritis Res 4, 30-35 (2002)

36. Arthur Veis: Mineralization in organic matrix frameworks. Rev Miner Geochem 54, 249-289 (2003)

37. G. N. Ramachandran, Gopinath Kartha: Structure of collagen. Nature 174, 269-279 (1954)

38. Alan J. Hodge, John A. Petruska: Recent studies with the electron microscope on ordered aggregates of the tropocollagen molecules. In: Aspects of protein structure. Ed: Ramachandran G N, Academic Press, London (1963)

39. Alan J. Hodge, John A. Petruska, Alan J. Bailey: The subunit structure of the tropocollagen macromolecule and its relation to various ordered aggregation states. In: Structure and function of connective and skeletal tissue. Eds: Jackson S F, Harkness R D, Partridge S M, Tristram G R, Butterworths, London (1965)

40. Desmond R. Cooper, Allan E. Russell: Intra- and intermolecular crosslinks in collagen in tendon, cartilage and bone. Clin Orthop Relat Res 67, 188-209 (1969)

41. Marvin L. Tanzer: Cross-linking of collagen. Endogenous aldehydes in collagen react in several ways to form a variety of unique covalent cross-links. Science 180, 561-566 (1973)

42. Lynda Knott, Alan J. Bailey: Collagen cross-links in mineralizing tissues: a review of their chemistry, function and clinical relevance. Bone 22, 181-187 (1998)

43. Melvin J. Glimcher, Elton P. Katz: The organization of collagen in bone: the role of noncovalent bonds in the relative insolubility of bone collagen. J Ultrastruct Res 12, 705-729 (1965)

44. Maria-Grazia Ascenzi, Antonio Ascenzi, Alessandro Benvenuti, Manfred Burghammer, Silvia Panzavolta, Adriana Bigi: Structural differences between "dark" and "bright" isolated human osteonic lamellae. J Struct Biol 141, 22-33 (2003)

45. A. Michael Parfitt, Marc K. Drezner, Francis H. Glorieux, John A. Kanis, Hartmut Malluche, Pierre J. Meunier, Susan M. Ott, Robert R. Recker: Bone histomorphometry: standardization of nomenclature, symbols, and units. J Bone Miner Res 2, 595-610 (1987)

46. Ermanno Bonucci, Guiliana Silvestrini: Ultrastructure of the organic matrix of embryonic avian bone after en bloc reaction with various electron-dense 'strains'. Acta Anat 156, 22-33 (1996)

47. Antonio Ascenzi, C. François, D. Steve Bocciarelli: On the bone induced by estrogen in birds. J Ultrastruct Res 8, 491-505 (1963)

48. Ermanno Bonucci, G. Gherardi: Histochemical and electron microscope investigations on medullary bone. Cell Tissue Res 163, 81-97 (1975)

49. Maria-Grazia Ascenzi, Antonio Benvenuti, Antonio Assenzi: Single osteon micromechanical testing. In: Mechanical testing of bone and the bone-implant interface. Eds: An Y H, Draughn R A, CRC Press, Boca Raton (2000)

50. Betty Nusgens, Alex Chantraine, Charles M. Lapiere: The protein in the matrix of bone. Clin Orthop Relat Res 88, 252-274 (1972)

51. A. G. Leaver, James T. Triffitt, Ian B. Holbrook: Newer knowledge of non-collagenous protein in dentin and cortical bone matrix. Clin Orthop Relat Res 110, 269-292 (1975)

52. John D. Termine, Alain B. Belcourt, Kathleen M. Conn, Hynda K. Kleian: Mineral and collagen-binding proteins of fetal calf bone. J Biol Chem 256, 10403-10408 (1981)

53. William T. Butler: Matrix macromolecules of bone and dentin. Coll Relat Res 4, 297-307 (1984)

54. William T. Butler: Noncollagenous proteins of bone and dentin: a brief overview. In: Chemistry and biology of mineralized tissues. Eds: Goldberg M, Boskey A, Robinson C, American Academy of Orthopaedic Surgeons, Rosemont, IL (2000)

55. Adele L. Boskey: Noncollagenous matrix proteins and their role in mineralization. Bone Miner 6, 111-123 (1989)

56. Adele L. Boskey: Biomineralization: conflicts, challenges and opportunities. J Cell Biochem 30/31, 83-91 (1998)

57. Paolo Bianco: Ultrastructural immunohistochemistry of noncollagenous proteins in calcified tissues. In: Ultrastructure of skeletal tissues. Eds: Bonucci E, Motta P M, Kluwer Academic Publishers, Boston (1990)

58. Marian F. Young, Janet M. Kerr, Kyomi Ibaraki, Anne-Marie Heegaard, Pamela Gehron Robey: Structure, expression, and regulation of the major noncollagenous matrix proteins of bone. Clin Orthop Relat Res 281, 275-294 (1992)

59. Ronald T. Ingram, Bart L. Clarke, Larry W. Fisher, Lorraine A. Fitzpatrick: Distribution of noncollagenous proteins in the matrix of adult human bone: evidence of anatomic and functional heterogeneity. J Bone Miner Res 8, 1019-1029 (1993)

60. Pamela G. Robey: Vertebrate mineralized matrix proteins: structure and function. Connect Tissue Res 35, 131-136 (1996)

61. Antonio Nanci: Content and distribution of noncollagenous matrix proteins in bone and cementum: relationship to speed of formation and collagen packing density. J Struct Biol 126, 256-269 (1999)

62. A. de Ricqlès, F. J. Meunier, J. Castanet, H. Francillon-Vieillot: Comparative microstructure of bone. In: Bone, Vol. 3: Bone matrix and bone specific products. Ed: Hall B K, CRC Press, Boca Raton (1991)

63. Paolo Bianco: Structure and mineralization of bone. In: Calcification in biological systems. Ed: Bonucci E, CRC Press, Boca Raton (1992)

64. Rachael V. Sugars, Anna M. Milan, John O. Brown, Rachel J. Waddington, Recce C. Hall, Graham Embery: Molecular interaction of recombinant decorin and biglycan with type I collagen influences crystal growth. Connect Tissue Res 44, 189-195 (2003)

65. Kazuto Hoshi, Shinichi Kemmotsu, Yasuhiro Takeuchi, Norio Amizuka, Hidehiro Ozawa: The primary calcification in bones follows removal of decorin and fusion of collagen fibrils. J Bone Miner Res 14, 273-280 (1999)

66. Gastone Marotti, Massimo Ferretti, F. Remaggi, Camilla Palumbo: Quantitative evaluation on osteocyte canicular density in human secondary osteons. Bone 16, 125-128 (1995)

67. Elisabeth M. Aarden, Peter J. Nijweide, Anja van der Plas, Marcel J. Alblas, Eleanor J. Mackie, Michael A. Horton, Miep H. Helfrich: Adhesive properties of isolated chick osteocytes *in vitro*. Bone 18, 305-313 (1996)

68. Elisabeth H. Burger, Jenneke Klein-Nulend, Arie van der Plas, Peter J. Nijweide: Function of osteocytes in bone - their role in mechanotransduction. J Nutr 125, 2020S-2023S (1995)

69. Elisabeth H. Burger, Jenneke Klein-Nulend: Mechanotransduction in bone - role of the lacuno-canalicular network. Faseb J 13, S101-112 (1999)

70. T. S. Gross, S. E. Warner: Bone. In: Encyclopedia of Neuroscience. Eds: Binder M D, Hirokawa N, Windhorst U, Springer, Berlin (2009)

71. Roberto Civitelli: Cell-cell communication in the osteoblast/osteocyte lineage. Arch Biochem Biophys 473, 188-192 (2008)

72. Manuel P. Mark, Charles W. Prince, Steffen Gay, Ronald L. Austin, Merra Bhown, Richard D. Finkelman,

William T. Butler: A comparative immunocytochemical study on the subcellular distributions of 44 kDa bone phosphoprotein and bone γ-carboxyglutamic acid (Gla)-containing protein in osteoblasts. J Bone Miner Res 2, 337-346 (1987)

73. Boris Sommer, Markus Bickel, Walter Hofstetter, Antoinette Wetterwald: Expression of matrix proteins during the development of mineralized tissues. Bone 19, 371-380 (1996)

74. Carlton G. Bellows, S. Reimers, Johan N. M. Heersche: Expression of mRNAs for type-I collagen, bone sialoprotein, osteocalcin, and osteopontin at different stages of osteoblastic differentiation and their regulation by 1,25 dihydroxyvitamin D3. Cell Tissue Res 297, 249-259 (1999)

75. Peter V. Hauschka, Frank H. Wians Jr: Osteocalcin-hydroxyapatite interaction in the extracellular organic matrix of bone. Anat Rec 224, 180-188 (1989)

76. Jean Menanteau, William F. Neuman, Margaret W. Neuman: A study of bone proteins which can prevent hydroxyapatite formation. Metab Bone Dis Rel Res 4, 157-162 (1982)

77. James T. Ninomiya, Russell P. Tracy, James D. Calore, Mark A. Gendreau, Robert J. Kelm, Kenneth G. Mann: Heterogeneity of human bone. J Bone Miner Res 5, 933-938 (1990)

78. Jeff P. Gorski: Is all bone the same? Distinctive distributions and properties of non-collagenous matrix proteins in lamellar vs. woven bone imply the existence of different underlying osteogenic mechanisms. Crit Rev Oral Biol Med 9, 201-223 (1998)

79. Cathy S. Carlson, Hermina M. Tulli, Manuel J. Jayo, Richard F. Loeser, Russell P. Tracy, Kenneth G. Mann, Michael R. Adams: Immunolocalization of noncollagenous bone matrix proteins in lumbar vertebrae from intact and surgically menopausal cynomolgus monkeys. J Bone Miner Res 8, 71-81 (1993)

80. Caren M. Gundberg: Biology, physiology, and clinical chemistry of osteocalcin. J Clin Ligand Assay 21, 128-138 (1998)

81. Adele L. Boskey, Frank H. Wians Jr, Peter V. Hauschka: The effect of osteocalcin on *in vitro* lipid-induced hydroxyapatite formation and seeded hydroxyapatite growth. Calcif Tissue Int 37, 57-62 (1985)

82. Paul A. Price, Matthew K. Williamson, Yoko Otawara: Characterization of matrix Gla protein. A new vitamin K-dependent protein associated with the organic matrix of bone. In: The chemistry and biology of mineralized tissues. Ed: Butler W T, Ebsco Media, Birmingham, Al (1985)

83. Guangbin Luo, Patricia Ducy, Marc D. McKee, Gerald J. Pinero, Evelyne Loyer, Richard R. Behringer, Gerard Karsenty: Spontaneous calcification of arteries and cartilage in mice lacking GLA protein. Nature 386, 78-81 (1997)

84. Kristina I. Boström: Cell differentiation in vascular calcification. Z Kardiol 89, 69-74 (2000)

85. Kristina Boström: Insights into the mechanism of vascular calcification. Am J Cardiol 88, 20E-22E (2001)

86. Sharif El-Maadawy, Mari T. Kaartinen, Thorsten Schinke, Monzur Murshed, Gerard Karsenty, Marc D. McKee: Cartilage formation and calcification in arteries of mice lacking matrix Gla protein. Connect Tissue Res 44, 272-278 (2003)

87. Paul A. Price, Matthew K. Williamson: Primary structure of bovine matrix Gla protein, a new vitamin K-dependent bone protein. J Biol Chem 260, 14971-14975 (1985)

88. William T. Butler, S. Sato, F. Rahemtulla, C. W. Prince, M. Tomana, M. Bhown, M. T. Dimuzio and A. L. J. J. Bronckers: Glycoproteins of bone and dentin. In: The chemistry and biology of mineralized tissues. Ed: Butler W T, EBSCO Media, Birmingham (1985)

89. Larry W. Fisher, John D. Termine: Noncollagenous proteins influencing the local mechanisms of calcification. Clin Orthop Relat Res 200, 362-385 (1985)

90. John D. Termine: The tissue specific proteins of the bone matrix. In: The chemistry and biology of mineralized tissues. Butler W T, EBSCO Media, Birmingham, AL (1985)

91. Arthur Veis: Phosphoproteins of dentin and bone. Do they have a role in matrix mineralization. In: The chemistry and biology of mineralized tissues. Ed: Butler W T, EBSCO Media, Birmingham, AL (1985)

92. Jeffrey P. Gorski: Acidic phosphoproteins from bone matrix: a structural rationalization of their role in mineralization. Calcif Tissue Int 50, 391-396 (1992)

93. M. S. Mackey, Mark L. Stevens, Deb C. Ebert, D. L. Tressler, K. S. Combs, C. K. Lowry, Paul N. Smith, J. E. McOsker: The ferret as a small animal model with BMU-based remodeling for skeletal research. Bone 17, 191S-196S (1995)

94. Christopher P. Jerome, Cynthia S. Johnson, Chris J. Lees: Effect of treatment for 3 months with human parathyroid hormone 1–34 peptide in ovariectomized cynomolgus monkeys (Macaca fascicularis). Bone 17, 415S-420S (1995)

95. Jun Inoue: Bone changes with long-term administration of low doses of 1–34 human PTH in adult beagles. J Jap Orthop Assoc 59, 409-427 (1985)

96. Rogely W. Boyce, Carol L. Paddock, Alan F. Franks, Maryann L. Jankowsky, Erik F. Eriksen: Effects of

intermittent hPTH (1–34) alone and in combination with 1,25 (OH)2D3 or risedronate on endosteal bone remodeling in canine cancellous and cortical bone. J Bone Miner Res 11, 600–613 (1996)

97. Pierre D. Delmas, Philippe Vergnaud, Monique E. Arlot, Philippe Pastoureau, Pierre J. Meunier, M. H. Nilssen: The anabolic effect of human PTH (1–34) on bone formation is blunted when bone resorption is inhibited by the bisphosphonate tiludronate - is activated resorption a prerequisite for the *in vivo* effect of PTH on formation in a remodeling system? Bone 16, 603-610 (1995)

98. Paolo Bianco, Pamela Gehron Robey: Marrow stromal stem cells. J Clin Invest 105, 1663-1668 (2000)

99. D. G. Carlström: Some aspects of the ultrastructure of bone. J Bone Joint Surg Am 39, 622-624 (1957)

100. Alan Boyde, Paolo Bianco, Michele Portigliatti Barbos, Antonio Ascenzi: Collagen orientation in compact bone: I. A new method for the determination of the proportion of collagen parallel to the plane of compact bone sections. Metab Bone Dis & Rel Res 5, 299-307 (1984)

101. Timothy G. Bromage, Haviva M. Goldman, Shannon C. McFarlin, Johanna Warshaw, Alan Boyde, Christopher M. Riggs: Circularly polarized light standards for investigations of collagen fiber orientation in bone. Anat Rec 274B, 157-168 (2003)

102. Rodolfo Amprino, Ake Engström: Studies on x-ray absorption and diffraction of bone tissue. Acta Anat 15, 1-22 (1952)

103. Antonio Ascenzi, Ermanno Bonucci, D. Steve Bocciarelli: Quantitative analysis of calcium in bone with a microradiographic method. Nuovo Cimento Series X 18, 216-220 (1960)

104. R. E. Rowland, Jenifer Josey, James H. Marshall: Microscopic metabolism of calcium in bone. III. Microradiographic measurements of mineral density. Radiat Res 10, 234-242 (1959)

105. Mitchell B. Schaffler, David B. Burr, Richard G. Fredrickson: Morphology of the osteonal cement line in human bone. Anat Rec 217, 223-228 (1987)

106. X. Neil Dong, Xiaohui Zhang, X. Edward Guo: Interfacial strength of cement lines in human cortical bone. Mech & Chem Biosys 2, 63-68 (2005)

107. John G. Skedros, Jennifer L. Holmes, Eric G. Vajda, Roy D. Bloebaum: Cement lines of secondary osteons in human bone are not mineral-deficient: new data in a historical perspective. Anat Rec Part A, 286, 781-803 (2005)

108. Alessandra Battaglia, F. Bruin, A Gozzini: Microwave apparatus for the measurement of the refraction dispersion and absorption of gases at relatively high pressure. Nuovo Cimento 7, 1 (1958)

109. Antonio Ascenzi, Antonio Benvenuti, Ermanno Bonucci: The tensile properties of single osteonic lamellae: technical problems and preliminary results. J Biomech 15, 29-37 (1982)

110. Antonio Ascenzi, Ermanno Bonucci: Relationship between ultrastructure and "pin test" in osteons. Clin Orthop Rel Res 121, 275-294 (1976).

111. Antonio Ascenzi, Paolo Baschieri, Antonio Benvenuti: The bending properties of single osteons. J Biomech 23, 763-771 (1990)

112. Peter Frasca, Richard A. Harper, J. Lawrence Katz: Isolation of single osteons and osteon lamellae. Acta Anat 95, 122-129 (1976)

113. Peter Frasca, Richard A. Harper, J. Lawrence Katz: Strain and frequency dependence of shear storage modulus for human single osteons and cortical bone microsample-size and hydration effects. J Biomech 14, 679-690 (1981)

114. Antonio Ascenzi, Ermanno Bonucci: The shearing properties of single osteons. Anat Rec 172, 499-510 (1972)

115. Antonio Ascenzi, Antonio Benvenuti, Francesco Mango, R. Simili: Mechanical hysteresis loops from single osteons: technical devices and preliminary results. J Biomech 18, 391-398 (1985)

116. Maria-Grazia Ascenzi, Mariasevera Di Comite, Plamen Mitov, John Michael Kabo: Hysteretic pinching of human secondary osteons subjected to torsion. J Biomech 40, 2619-2627 (2007)

117. Maria-Grazia Ascenzi, Alexandre Lomovtsev: Collagen orientation patterns in human secondary osteons, quantified in the radial direction by confocal microscopy. J Str Biol 153, 14-30 (2006)

118. Maria-Grazia Ascenzi, Jaya Gill, Alexander Lomovtsev: Collagen orientation patterns around osteocyte lacunae in human secondary osteons by confocal microscopy. J Biomech 41, 3428-3437 (2008)

119. G. R. Price, S. Schwartz: Fluorescence microscopy. In: Physical Techniques in Biological Research, Vol. 3. Eds: Oister G, Pollister A W, Academic Press, New York (1956)

120. H. S. Allen: Photo-elasticity. Longmans Green, London (1925)

121. A. I. D. Prentice: Autofluorescence of bone tissues. J Clin Pathol 20, 717–719 (1967)

122. Dido Yova, Vladimir Hovhannisyan, Theodossis Theodossiou: Photochemical effects and hypericin photosensitizied processes in collagen. J Biomed Opt 6,

52–57 (2001)
123. Alan Boyde, M. H. Hobdell: Scanning electron microscopy of lamellar bone. Z Zellforsch 93, 213–231 (1969)

124. Haviva M. Goldman, Timothy G. Bromage, Christopher D. L. Thomas, John G. Clement: Relationships among microstructural properties of bone at the human midshaft femur. J Anat 206, 127-139 (2005)

125. Eve Donnelly, Rebecca M. Williams, Seth A. Downs, Michelle E. Dickinson, Shefford P. Baker, Marjolein C. H. van der Meulen: Quasistatic and dynamic nanomechanical properties of cancellous bone tissue relate to collagen content and organization. J Mater Res 21, 2106-2117 (2006)

126. Antonio Ascenzi, Alessandro Benvenuti: Orientation of collagen fibers at the boundary between two successive osteonic lamellae and its mechanical interpretation. J Biomech 19, 455-463 (1986)

127. Alan Boyde: Methodology of calcified tissue specimen preparation for scanning electron microscopy. In: Methods of Calcified Tissue Preparation. Ed: Dickson G R, Elsevier Science Publishers B.V., Amsterdam (1984)

128. Alan Boyde, Sheila J. Jones: Scanning electron microscopy of bone: Instrument, specimen, and issues. Mic Res Tech 33, 92-120 (1996)

129. Peter Frasca, Richard A. Harper, J. Lawrence Katz: Mineral and collagen fiber orientation in human secondary osteons. J Dental Res 57, 526-533 (1978)

130. Elena I. Suvorova, Pavel P. Petrenko, Philippe A. Buffat: Scanning and transmission electron microscopy for evaluation of order/disorder in bone structure. Scanning 29, 162-170 (2007)

131. Gastone Marotti, M. A. Muglia, Camilla Palumbo: Structure and function of lamellar bone. Clin Rheum 13, 63-68 (1994)

132. Todd M. Boyce, Roy D. Bloebaum, Kent N. Bachus, John G. Skedros: Reproducible method for calibrating the backscattered electron signal for quantitative assessment of mineral content in bone. Scan Micro 4, 591-603 (1990)

133. R. D. Crofts, Todd M. Boyce, Roy D. Bloebaum: Aging changes in the osteon mineralization in the human femoral neck. Bone 15, 147-152 (1994)

134. David M. Cooper, C. David Thomas, John G. Clement, Andrei L. Turinsky, Christoph W. Sensen, Benedikt Hallgrmsson: Age-dependent change in the 3D structure of cortical porosity at the human femoral midshaft. Bone 40, 957-965 (2007)

135. David W. Dempster, Felicia Cosman, Etah S. Kurland, Hua Zhou, Jeri Nieves, Lillian Woelfert, Elizabeth Shane, Katarina Plavetić, Ralph Müller, John Bilezikian, Robert Lindsay: Effects of daily treatment with parathyroid hormone on bone microarchitecture and turnover in patients with osteoporosis: a paired biopsy study. J Bone Miner Res 16, 1846-1853 (2001)

136. Philippe K. Zysset, X. Edward Guo, C. Edward Hoffler, Kristin E. Moore, Steven A. Goldstein: Elastic modulus and hardness of cortical and trabecular bone lamellae measured by nanoindentation in the human femur. J Biomech 32, 1005-1012 (1999)

137. Rachel C. Paietta, Sara E. Campbell, Virginia L. Ferguson: Influences of spherical tip radius, contact depth and contact area on nanoindentation properties of bone. J Biomech 44, 285-290 (2011)

138. Ji Young Rho, Peter Zioupos, John D. Currey, George M. Pharr: Microstructural elasticity and regional heterogeneity in human femoral bone of various ages examined by nano-indentation. J Biomech 35, 189-198 (2002)

139. Antonio Ascenzi, Ermanno Bonucci, D. Steve Bocciarelli: An electron microscope study on primary periosteal bone. J Ultrastr Res 18, 605-618 (1966)

140. Ariel Simkin, Gautier Robin: Fracture formation in differing collagen fiber pattern in compact bone. J Biomech 7, 183-188 (1974)

141. R. Bruce Martin, David B. Burr, Neil A. Sharkey: Skeletal Tissue Mechanics. Springer, New York (1998)

142. Gwendolen C. Reilly: Observations of microdamage around osteocyte lacunae in bone. J Biomech 33, 1131-1134 (2000)

143. Michele Portigliatti-Barbos, Paolo Bianco, Antonio Ascenzi, Alan Boyde: Collagen orientation in compact bone: II. Distribution of lamellae in the whole of the human femoral shaft with reference to its mechanical properties. Met Bone Dis & Rel Res 5, 309-315 (1984)

144. Mario Raspanti, Stefano Guizzardi, Rita Strocchi, Andrea Ruggeri: Collagen fibril patterns in compact bone: preliminary ultrastructural observations. Acta Anat 155, 249-255 (1996)

145. Luca Cristofolini, Fulvia Taddei, Massimiliano Baleani, Fabio Baruffaldi, Susanna Stea, Marco Viceconti: Multiscale investigation of the functional properties of the human femur. Philos Transact A Math Phys Eng Sci 366, 3319-3341 (2008)

146. Alina Beraudi, Susanna Stea, M. Montesi, Massimiliano Baleani, Marco Viceconti: Collagen orientation in human femur, tibia and fibula shaft by circularly polarized light. Bone 44, S320 (2009)

147. Alina Beraudi, Susanna Stea, Barbara Bordini, Massimiliano Baleani, Marco Viceconti: Osteon classification in human fibular shaft by circularly polarized

light. Cells Tissues Organs 191, 260-268 (2010)
148. Christopher M. Riggs, L. C. Vaughan, G. Paul Evans, L. E. Lanyon, Alan Boyde: Mechanical implications of collagen fibre orientation in cortical bone of the equine radius. Anat Embryol 187, 239-248 (1993)

149. Sophi S. Ionova-Martin, Sun-Hee Do, Hans Dieter Barth, M. Szadkowska, Alexandra E. Porter, Joel W. Ager III, Joel W. Ager Jr, Tamara Alliston, Christian Vaisse, Robert O. Ritchie: Reduced size-independent mechanical properties of cortical bone in high-fat diet-induced obesity. Bone 46, 217-225 (2010)

150. John D. Currey: Three analogies to explain the mechanical properties of bone. Biorheology 2, 1-10 (1964)

151. John D. Currey: The relationship between the stiffness and the mineral content of bone. J Biomech 2, 477-480 (1969)

152. J. Lawrence Katz: Composite material models for cortical bone. In: Mechanical Properties of Bone. Ed: Cowin S C, The American Society of Mechanical Engineers, New York (1981)

153. Marie-Madeleine Giraud-Guille, Laurence Besseau, Raquel Martin: Liquid crystalline assemblies of collagen in bone and *in vitro* systems. J Biomech 36, 1571-1579 (2003)

154. Harry A. Hogan: Micromechanics modeling of Haversian cortical bone properties. J Biomech 25, 549-556 (1992)

155. Ramana M. V. Pidaparti, David B. Burr: Collagen fiber orientation and geometry effects on the mechanical properties of secondary osteons. J Biomech 29, 869-880 (1992)

156. H. Daniel Wagner, Steve Weiner: On the relationship between the microstructure of bone and its mechanical stiffness. J Biomech 25, 1311-1320 (1992)

157. Boujemaa Aoubiza, Jean Marie Crolet, Anne Meunier: On the mechanical characterization of compact bone structure using homogenization theory. J Biomech 29, 1539-1547 (1996)

158. Udi Akiva, H. Daniel Wagner, Steve Weiner: Modeling the three-dimensional elastic constants of parallel-fibred and lamellar bone. J Mat Sci 33, 1497-1509 (1998)

159. Steve Weiner, Wolfie Traub, H. Daniel Wagner: Lamellar bone: structure-function relations. J Struct Biol 126, 241-255 (1999)

160. Ingomar Jäger, Peter Fratzl: Mineralized collagen fibrils: A mechanical model with staggered arrangement of mineral particles. Biophysics J 79, 1737-1746 (2000)

161. Shiva P. Kotha, Nejat Guzelsu: Modeling the tensile mechanical behavior of bone along the longitudinal direction. J Theor Biol 219, 269-279 (2002)
162. Iwona Jasiuk, Martin Ostoja-Starzewski: Modeling of bone at single lamella level. Biomech Mod Mechan 3, 67-74 (2004)

163. Ani Ural, Peter Zioupos, Drew Buchanan, Deepak Vashishth: The effect of strain rate on fracture toughness of human cortical bone: A finite element study. J Mech Behavior Biom Mat, online (2011)

164. Zhen-bing Cai, Shan-shan Gao, Min-hao Zhu, Juan Liu, Huo-ming Shen, Hai-yang Yu, Zhong-rong Zhou: Investigation of micro-cracking behaviors of human femur cortical bone during radial fretting. Tribology Inter, online (2010)

165. Melissa L. Knothe Tate: Top down and bottom up engineering of bone. J Biomech 44, 304-312 (2011)

166. Daan Waanders, Dennis Janssen, Kenneth A. Mann, Nico Verdonschot: The behavior of the micro-mechanical cement-bone interface affects the cement failure in total hip replacement. J Biomech 44, 228-234 (2011)

167. Stephen C. Cowin: Bone Mechanics Handbook. CRC Press, New York (2001)

168. Romaine R. Bruns, Jerome Gross: High-Resolution analysis of the modified quarter-stagger model of the collagen fibril. Biopolymers 13, 931-941 (1974)

169. Barbara Riemer McCreadie, Scott J. Hollister: Strains concentration surrounding an ellipsoidal model of lacunae and osteocytes. Computer Methods. Biomech Biom Eng 1, 61-68 (1997)

170. Daniel P. Nicolella, Donald E. Moravits, Adrian M. Gale, Lynda F. Bonewald, James Lankford: Osteocyte lacunae tissue strain in cortical bone. J Biomech 39, 1735-1743 (2006)

171. Amber Rath Bonivtch, Lynda F. Bonewald, Daniel P. Nicolella: Tissue strain amplification at the osteocyte lacuna: a microstructural finite element analysis. J Biomech 40, 2199-2206 (2007)

172. Patrick J. Prendergast, Rik Huiskes: Microdamage and osteocyte-lacuna strain in bone: A microstructural finite element analysis. J Biomech Eng-T ASME 118, 240-246 (1996)

173. Chris De Laet, Anders Oden, Helena Johansson, Olof Johnell, Bengt Jonsson, John A. Kanis: The impact of the use of multiple risk factors on case finding strategies: a mathematical framework. Osteop Inter 16, 313-318 (2005)

174. Luis Cardoso, Alain Meunier, Christian Oddou: *In vitro* acoustic wave propagation in human and bovine cancellous bone as predicted by the Biot's theory. J Mech Med Biol 8, 1-19 (2008)

175. Maria-Grazia Ascenzi, Neal Kawas, Joyce H. Keyak:

Patient-specific hierarchical simulation of proximal femur. 10th Int Conf Chem Biol Min Tissues, Scottsdale, Arizona, November 7-12 (2010)

176. Elham Hamed, Yikhan Lee, Iwona Jasiuk: Multiscale modeling of elastic properties of cortical bone. Acta Mech 213, 131–154 (2010)

177. Dennis Carter, Wilson C. Hayes: Compact bone fatigue damage - I. Residual strength and stiffness. J Biomech 10, 325-337 (1977)

178. Dennis Carter, Wilson C. Hayes: Fatigue life of compact bone - I effects of stress amplitude, temperature and density. J Biomech 9, 27-34 (1976)

179. Dennis Carter, Wilson C. Hayes, David J. Schurman: Fatigue life of compact bone - II. Effects of microstructure and density. J Biomech 9, 211-218 (1976)

180. Dennis Carter, Dan M. Spengler: Mechanical Properties and Composition of Cortical Bone. Clin Orthop Rel Res 135, 192-217 (1978)

181. W. Haynes, Dennis Carter: Biomechanics of bone. In: Skeletal research: an experimental approach. Eds: Simmons D J, Kunin A S, Academics Press Inc, New York (1979)

182. Dennis R. Carter, William E. Caler, Dan M. Spengler, Victor H. Frankel: Fatigue behavior of adult cortical bone: the influence of mean strain and strain range. Acta Orthop 52, 481-490 (1981)

183. Roderic S. Lakes, J. Lawrence Katz: Viscoelastic properties of wet cortical bone - III. A nonlinear constitutive equation. J Biomech 12, 689-698 (1979)

184. Roderic S. Lakes: Letter to the Editor: On the torsional properties of single osteons. J Biomech 28, 1409 (1995)

185. Ahmad Raeisi Najafi, Ahmad Reza Arshi, Mohamad Reza Esiami, Shahriar Fariborz, Manssour H. Moeinzadeh: Micromechanics fracture in osteonal cortical bone: A study of the interactions between microcrack propagation, microstructure and the material properties. J Biomech 40, 2788-2795 (2007)

186. E. Weinan, Bjorn Engquist: Multiscale modeling and computation. Notices of the AMS, 50, 1062-1070 (2003)

187. Jochen Blath, Peter Mörters, Michael Scheutzow: Trends in Stochastic Analysis. London Math Soc Lecture Note Series 353, Cambridge University Press (2009)

188. Alexander K. Hartmann, Heiko Rieger: New Optimization Algorithms in Physics. Wiley-VCH Verlag GmbH & Co. KGaA, Weinheim, Germany (2004)

189. Keith Devlin: Mathematics: The Science of Patterns: The Search for Order in Life, Mind and the Universe. Scientific American Paperback Library, New York, NY (1996)

190. Gi Chung, Triet M. Le, Linh H. Lieu, Nicolay M. Tanushev, Luminita A. Vese: Computational methods for image restoration, image segmentation, and texture modeling. In: Computational Imaging IV, Proc. of SPIE-IS&T Electronic Imaging. Eds: Bouman C A, Miller E L, Pollak I, SPIE, Bellingham, Washington (2006)

191. C. L. Y. Yeong, Salvatore Torquato: Reconstructing random media. Phys Rev E 57, 495-506 (1998)

192. Javier Portilla, Eero P. Simoncelli: A parametric texture model based on joint statistics of complex wavelet coefficients. Int J Comp Vision 40, 49-71 (2000)

193. Carlos Bonifasi-Lista, Elena Cherkaev: Analytical relations between effective material properties and microporosity: Application to bone mechanics. Int J Eng Science 46, 1239-1252 (2008)

194. Herbert Edelsbrunner, Ernst Mücke: Three-dimensional alpha shapes. ACM Trans Graph 13, 43-72 (1994)

195. Kenneth M. Golden, Hajo Eicken, A. L. Heaton, J. Miner, Daniel Pringle, J. J. Zhu: Thermal evolution of permeability and microstructure in sea ice. Geophys Res Letters 34, L16501-L16506 (2007)

196. Kenneth M. Golden, N. Benjamin Murphy, Elena Cherkaev: Spectral analysis and connectivity of porous microstructures in bone. J Biomech 44, 337-344 (2011)

197. Joyce H. Keyak, Stephen A. Rossi: Prediction of femoral fracture load using finite element models: an examination of stress- and strain-based failure theories. J Biomech 33, 209-214 (2000)

198. J. Ghanbari, R. Naghdabadi: Nonlinear hierarchical multiscale modeling of cortical bone considering its nanoscale microstructure. J Biomech 42, 1560-1565 (2009)

199. Melissa L. Knothe Tate: Multi-scale computational engineering of bones: state of the art insights for the future. In: Engineering of Functional Skeletal Tissues. Eds: Bronner F, Farach-Carson C, Mikos A, Springer-Verlag, London (2007)

200. David Green, Declan Walsh, Stephen Mann, Richard O. C. Oreffo: The potential of biomimesis in bone tissue engineering: lessons from the design and synthesis of invertebrate skeletons. Bone 6, 810-815 (2002)

201. Micah R. Rogel, Hongjin Qiu, Guillermo A. Ameer: The role of nanocomposites in bone regeneration. Mater Chem 18, 4233-4241 (2008)

202. Marcel Smid, Yixin Wang, Jan G. M. Klijn, Anieta M. Sieuwerts, Yi Zhang, David Atkins, John W. M. Martens, John A. Foekens: Genes associated with breast cancer metastatic to bone. J Clin Oncology 24, 2261-

2267 (2006)

203. Scott J. Hollister, R. D. Maddox, Juan M. Taboas: Optimal design and fabrication of scaffolds to mimic tissue properties and satisfy biological constraints. Biomaterials 20, 4095-4103 (2002)

204. Cheng Yu Lin, Noboru Kikuchi, Scott J. Hollister: A novel method for biomaterial scaffold internal architecture design to match bone elastic properties with desired porosity. J Biomech 5, 623-636 (2004)

205. Roger M. Zebaze, Ali Ghasem Zadeh, Ann Bohte, Sandra Iuliano-Burns, Michiko Mirams, Roger Ian Price, Eleanor J. Mackie, Ego Seeman: Intracortical remodelling and porosity in the distal radius and post-mortem femurs of women: a cross-sectional study. Lancet 375, 1729-1736 (2010)

206. Eve Donnelly, Dennis S. Meredith, Brian P. Gladnick, Brian J. Rebolledo, J. M. Lane, Adele L. Boskey: Reduced bone tissue heterogeneity with bisphosphonate treatment in postmenopausal women with fractures. Poster, 56th Annual Meeting of ORS (2010)

207. Elizabeth Shane, David Burr, Peter R. Ebeling, Bo Abrahamsen, Robert A. Adler, Thomas D. Brown, Angela M. Cheung, Felicia Cosman, Jeffrey R. Curtis, Richard Dell, David Dempster, Thomas A. Einhorn, Harry K. Genant, Piet Geusens, Klaus Klaushofer, Kenneth Koval, Joseph M. Lane, Fergus McKiernan, Ross McKinney, Alvin Ng, Jeri Nieves, Regis O'Keefe, Socrates Papapoulos, Howe Tet Sen, Marjolein C. H. van der Meulen, Robert S. Weinstein, Michael Whyte: Atypical subtrochanteric and diaphyseal femoral fractures: report of a task force of the American Society for Bone and Mineral Research. J Bone Min Res 25, 2267-2294 (2010)

208. Samuel Gourion-Arsiquaud, Matthew R. Allen, David B. Burr, Deepak Vashishth, Simon Y. Tang, Adele L. Boskey: Bisphosphonate treatment modifies canine bone mineral and matrix properties and their heterogeneity. Bone 46, 666-672 (2010)

209. Babul Borah, Tom Dufresne, Joe Nurre, Roger Phipps, Paula Chmielewski, Leigh Wagner, Mark Lundy, Mary Bouxsein, Roger Zebaze, Ego J. Seeman: Risedronate reduces intracortical porosity in women with osteoporosis. Bone Miner Res 25, 41-47 (2010)

210. Jonathan Reeve, Geoffrey W. Tregear, John A. Parsons: Preliminary trial of low doses of human parathyroid 1-34 peptide in treatment of osteoporosis. Clin Endocrinol 21, 469-477 (1976)

211. Jonathan Reeve, Pierre J. Meunier, John A. Parsons, Michel Bernat, Olav L. M. Bijvoet, Philippe Courpron, Claude Edouard, Leslie Klenerman, Robert M. Neer, Jean C. Renier, David Slovik, F. Jon F. E. Vismans, John T. Potts: Anabolic effect of human parathyroid hormone fragment on trabecular bone in involutional osteoporosis: A multicentre trial. Br Med J 280, 1340-1344 (1980)

212. David M. Slovik, Daniel I. Rosenthal, Samuel H. Doppelt, John T. J. Potts, Margaret A. Daly, Julie A. Campbell, Robert M. Neer: Restoration of spinal bone in osteoporotic men by treatment with human parathyroid hormone (1-84) and 1,25 dihydroxyvitamin. J Bone Miner Res 1, 377-381 (1986)

213. Joel S. Finkelstein, Anne Klibanski, Elizabeth H. Schaefer, Mark D. Hornstein, Issac Schiff, Robert M. Neer: Parathyroid hormone for the prevention of bone loss induced by estrogen deficiency. N Engl J Med 331, 1618-1623 (1994)

214. Robert Lindsay, Jeri Nieves, Carmelo Formica, Emily Henneman, Lillian Woelfert, Victor Shen, David Dempster, Felicia Cosman: Randomized controlled study of effect of parathyroid hormone on vertebral-bone mass and fracture incidence among postmenopausal women on oestrogen with osteoporosis. Lancet 350, 550-555 (1997)

215. Anthony B. Hodsman, Laurence J. Fraher, Peter H. Watson, Truls Ostbye, Larry W. Stitt, Jonathan D. Adachi, Donald H. Taves, Derek A. Drost: Randomized controlled trial to compare the efficacy of cyclical parathyroid hormone versus cyclical parathyroid hormone and sequential calcitonin to improve bone mass in postmenopausal women with osteoporosis. J Clin Endocrinol Metab 82, 620-628 (1997)

216. E. Bruce Roe, Sarah D. Sanchez, Aimee del Puerto, Pierina Bachetti, Christopher E. Cann, Claude D. Arnaud: Parathyroid hormone 1-34 (hPTH 1-34) and estrogen produce dramatic bone density increases in postmenopausal osteoporosis - results from a placebo-controlled randomized trial. J Bone Miner Res 14, S137 (1997)

217. Nancy E. Lane, Sarah Sanchez, Gunnar W. Modin, Harry K. Genant, Elena Pierini, Claude D. Arnaud: Parathyroid hormone can reverse corticosteroid induced osteoporosis. Results of a randomized controlled clinical trial. J Clin Invest 102, 1627-1633 (1998)

218. Felicia Cosman, Jeri Nieves, Carmelo Formica, Lillian Woelfert, Victor Shen, Robert Lindsay: Parathyroid hormone in combination with estrogen dramatically reduces vertebral fracture risk. Osteopor Int 11, S176 (2000)

219. Robert M. Neer, Claude D. Arnaud, Jose R. Zanchetta, Richard Prince, Gregory Gaich, Jean-Yves Reginster, Anthony B. Hodsman, Erik F. Eriksen, Sophia Ish-Shalom, Harry K. Genant, Ouhong Wang, Dan Mellstrom, Erik S. Oefjord, Ewa Marcinowska-Suchowierska, Jorma Salmi, Henk Mulder, Johan Halse, Andrzej Z. Sawicki, Bruce H. Mitlak: Effect of parathyroid hormone (1-34) on fractures and bone mineral density in postmenopausal women with osteoporosis. N Engl J Med 344, 1434-1441 (2001)

220. Chung-Ching Liu, Dike N. Kalu: Human parathyroid hormone (1–34) prevents bone loss and augments bone formation in sexually mature ovariectomized rats. J Bone

Miner Res 4, 449-458 (1990)

221. Toru Hirano, David B. Burr, Charles H. Turner, Masahiko Sato, Rick L. Cain, Janet M. Hock: Anabolic effects of human biosynthetic parathyroid hormone fragment (1-34), LY333334, on remodeling and mechanical properties of cortical bone in rabbits. J Bone Miner Res 14, 536-545 (1999)

222. Anthony B. Hodsman, Marcin Kisiel, Jonathan D. Adachi, Laurence J. Fraher, Peter H. Watson: Histomorphometric evidence of increased bone turnover without change in cortical thickness or porosity after 2 years of cyclical hPTH(1-34) therapy in women with severe osteoporosis. Bone 27, 311-318 (2000)

223. Gloria Rashid, Jaques Bernheim, Jack Green, Sydney Benchetrit: Parathyroid hormone stimulates the endothelial expression of vascular endothelial growth factor. Eur J Clin Invest 38, 798-803 (2008)

224. Jun Guo, Minlin Liu, Dehong Yang, Mary L. Bouxsein, Hiroaki Saito, R. J. Sells Galvin, Stuart A. Kuhstoss, Clare C. Thomas, Ernestina Schipani, Roland Baron, F. Richard Bringhurst, Henry M. Kronenberg: Suppression of Wnt signaling by Dkk1 attenuates PTH-mediated stromal cell response and new bone formation. Cell Metab 11, 161-171 (2010)

225. Chris Paszty, Charles H. Turner, Martyn K. Robinson: Sclerostin: a gem from the genome leads to bone-building antibodies. J Bone Min Res 25, 1897-1904 (2010)

226. Kathleen I. Pinson, Jane Brennan, Susan Monkley, Brian J. Avery, William C. Skarnes: An LDL receptor-related protein mediates Wnt signalling in mice. Nature 407, 535-538 (2000)

227. Elizabeth A. Wang, Vicki Rosen, Josephine S. D'Alessandro, Marc Bauduy, Paul Cordes, Tomoko Harada, David I. Israel, Rodney M. Hewick, Kelvin V. Kerns, Peter LaPan, Deborah P. Luxenberg, David Mcquaid, Ioannis K. Moutsatsos, John Nove, John M. Wozney: Recombinant human bone morphogenetic protein induces bone formation. Proc Nati Acad Sci 87, 2220-2224 (1990)

228. Maria-Grazia Ascenzi, Vivian P. Liao, Ben Minsuk Lee, Fabrizio Billi, Robert Lindsay, Felicia Cosman, Jeri W. Nieves, John P. Bilezikian, David W. Dempster: Short-term parathyroid hormone treatment improves cortical bone microstructure, Abstract, Research Day, Orthopeadic Hospital, Los Angeles (2011)

229. Jeremy Power, Nigel Loveridge, Andrew Lyon, Neil Rushton, Mike Parker, Jonathan Reeve: Bone remodeling at the endocortical surface of the human femoral neck: a mechanism for regional cortical thinning in cases of hip fracture. J Bone Miner Res 18, 1775-1780 (2003)

Abbreviations: OC: osteocalcin, MGP: matrix Gla-protein, CPL: circularly polarized light, TEM: transmission electron microscopy, SEM: scanning electron microscopy, STEM: scanning transmission electron microscope, microCT: micro computed tomography, BMD: bone mineral density, FE: finite element, DXA: dual energy X-ray absorptiometry.

Key Words: Bone, Finite element, Lacuna, Lamella, Mathematical model, Mechanical properties, micro-structure, Osteocyte, Seconday osteon, Review

Send correspondence to: Maria-Grazia Ascenzi, UCLA, Orthopaedic Hospital Department of Orthopaedic Surgery, University of California at Los Angeles, Rehabilitation Bldg 22-69, 1000 Veteran Avenue, Los Angeles, CA 90095, Tel: 310-825-6341, Fax: 310-825-5290, E-mail: mgascenzi@mednet.ucla.edu.

http://www.bioscience.org/current/vol17.htm